Forearc crustal faults as tsunami sources in the upper plate of the Lesser Antilles subduction zone. The Case study of the Morne Piton fault system.

Melody Philippon[1,*], Jean Roger[2], Jean-Frederic. Lebrun[1], Isabelle Thinon[3], Océane Foix[4], Stéphane Mazzotti[4], Marc-Andre Gutscher[5], Leny Montheil[4], Jean-Jacques Cornée[4].

1. Géosciences Montpellier, Université de Montpellier, CNRS, Université des Antilles, Pointe-à-Pitre, French West Indies.

2. Earth and Structure Processes Department, GNS Sciences, Lower Hutt, New Zealand.

3. BRGM – French Geological survey, 3 avenue Claude Guillemin 45060 Orléans

4. Géosciences Montpellier, Université de Montpellier, CNRS, Université des Antilles, Montpellier, France.

5. Geo-Ocean, Univ.Brest, CNRS, Ifremer, Brest, France.

* Corresponding author : melody.philippon@univ-antilles.fr

Abstract

In this study, alternatively to the megathrust, we identify upper plate normal faults orthogonal to the trench as a possible tsunami source along the Lesser Antilles subduction zone. The Morne Piton fault system, is such a trench-perpendicular upper crustal fault at the latitude of Guadeloupe. By the means of seismic reflection, high resolution bathymetry, remotely operated vehicle (ROV) imaging and dating, we reassess the slip rate of the Morne Piton fault since 7Ma, *i.e.* its inception, and quantify an average rate of 0.25 mm·yr^{-1} since ca. 1.2Ma dividing by two previous estimations and thus increasing the earthquake time recurrence and lowering the associated hazard. ROV dive revealed a metric scarp with striae at the toe of the Morne Piton fault system suggesting a recent fault rupture. We estimate a fault rupture area of $\sim$ 450-675 km^2 and then a magnitude range for a maximum seismic event around M_w 6.5 ± 0.5 making this fault potentially tsunamigenic as the nearby Les Saintes Fault responsible for a tsunami following the 2004, M_w 6.3 earthquake. Consequently, we simulate a multi-segment tsunami model representative for a worst-case scenario as if the whole identified Morne Piton fault segments ruptured together. Our model provides clues for the potential impact of local tsunamis on the surrounding coastal area as well as for local bathymetric controls

on tsunami propagation. We illustrate that (i) shallow water plateaus act as secondary sources and are responsible for a wrapping of the tsunami waves around the island of Marie-Galante, (ii) canyons indenting the shallow water plateau slope break are focusing and enhancing the wave height in front of the most touristic and populated town of the island, (iii) resonance phenomenon is observed within Les Saintes archipelago showing that the waves' frequency content is able to perturbate the sea-level during many hours after the seismic rupture.

Keywords: subduction zone, forearc, crustal fault, slip rate, tsunami hazard, Lesser Antilles, Guadeloupe Island

1. Introduction

Regions at the vicinity of active subduction zones are prone to seismic and related hazards, including tsunamis, exposing their inhabitants to multiple threats. Megathrust earthquakes represent the greatest threat with the highest seismic moments and consequently huge tsunamigenic potential (Satake and Tanioka, 1999). Earthquakes triggered on crustal faults in the overriding plate represent an additional hazard that needs to be quantified (Bilek, 2010). In order to assess the hazards and mitigate the risks associated with these crustal faults, it is essential to estimate their slip rates.

On land, slip rates on active faults are determined from paleo-seismic trenches (McCalpin, 1996), high resolution geophysical investigation (Wallace, 1981; Zhang et al., 2014), satellite imagery (Tronin, 2009), InSAR (Biggs and Wright, 2020), geodetic measurement (GNSS: Symithe et al., 2013) as well as seismicity which account for the present-day strain accumulation of the crust. Offshore, slip rate estimates are provided by the means of underwater geodesy (*i.e.* acoustic geodesy: Kido et al., 2006; Petersen et al., 2019; Fujita et al., 2006) or fiber optic monitoring (Hirata et al., 2002; Gutscher et al., 2019). The recurrence time of events may be estimated by the study of turbidite deposits cores (e.g., Cascades: Goldfinger et al., 2012; Taiwan: Lehu et al., 2016; Antilles: Seibert et al., 2020; New Zealand: Lewis, 1980), high resolution marine seismic and multibeam echo-sounder data (e.g., Escartín et al., 2016, 2018), and submarine dives survey (e.g., Geli et al., 2011). However, constraining hazard models in areas undergoing slow strain rates remains challenging as the earthquakes recurrence time overcomes the historical period. Indeed,

geodetic measurements require decades-long time series as the resolution of the method is not accurate enough and erosion or high sedimentation rates may have erased or covered, respectively, the active fault scarps making it difficult to identify active faults segments. Therefore, datasets based on the last ten to hundred years of record along tectonic systems undergoing slow strain rates may not be representative of the bulk strain and may be at the origin of biased estimations of slip rate along these faults.

The Lesser Antilles (Eastern Caribbean) records slow deformation rates as the north and south American tectonic plates slowly subduct under the Caribbean plate ($20 \text{mm} \cdot \text{yr}^{-1}$ - Figure 1). Extensional tectonics and normal faulting affect the forearc (Feuillet et al., 2002, De Min et al., 2015, Boucard et al., 2021) but available historical data do not report tsunami events related to forearc fault rupture. However, the Les Saintes M_w 6.3 earthquake of December 2004 ruptured the Roseau normal fault (Feuillet et al., 2011, Bazin et al., 2010). The earthquake reached an intensity up to VIII in the Guadeloupe Archipelago (Figure 1), being felt by most of its ~400,000 inhabitants, and was responsible for one casualty. This earthquake triggered a tsunami with up to 2 m high waves at the coast and a maximum measured run-up distance of 42 m in Les Saintes (Zahibo et al. 2005; Le Friant et al. 2008; Cordrie et al. 2020). Prior to this event, this fault was unmapped and therefore not identified as an active fault (Feuillet et al., 2002; Terrier and Combes, 2002). Forearc normal faults, similar to Les Saintes fault system, may pose a threat to the 4 million inhabitants of the Lesser Antilles that are living on volcanic arc islands facing the subduction trench to the east and literally sitting over the subduction interface.

The present study focuses on the Morne Piton fault system, perpendicular to the subduction trench, which is one of the most prominent onshore-offshore fault systems which cuts the Guadeloupe Archipelago arc and forearc islands (Figure 1). Regarding the seismic and tsunami hazards related to this fault system and the vulnerability of the coastal population and infrastructures of the archipelago, the objectives are to (1) estimate the fault slip rate (2) determine the geometry of the fault segments, and (3) model the associated tsunami hazard, since such a joint approach has been lacking so far. In the following study, the fault geometry is refined in order to provide an up-to-date map of the fault segments thanks to high-resolution (HR) bathymetric data. Then, we integrate its long-term slip rate over the last *ca.* 7 My, *i.e.* from fault initiation to present-day, by the mean of HR seismic reflection lines and available biostratigraphic and isotopic dates.

98   Secondly, Remotely Operated Vehicles (ROV) explorations of seafloor rupture allowed us

99   to measure the height of the fault scarp and to determine the fault kinematics from

100 striations observed along a recent co-seismic scarp. Because the overall geometry of this

101 fault system is comparable to the Les Saintes fault system in terms of length, seafloor

102 scarp and dip, we postulate that a rupture along the Morne Piton fault may trigger a local

103 tsunami close to the coasts of the Guadeloupe Archipelago. Therefore we study the

104 seismogenic and tsunamigenic potential of the Morne Piton fault system providing an

105 overview of what could happen in terms of tsunami generation if all the segments of the

106 Morne Piton fault ruptured simultaneously, *i.e.* a plausible worst-case scenario. This

107 scenario allows to identify and discuss the local bathymetric controls on the propagation

108 of the resulting tsunami wave and the consequences (*e.g.,* amplifications and

109 interferences) in near-shore areas of the neighboring populated islands. We do not assess

110 coastal inundation scenarios, as our scenario can't be refined by observational rupture

111 data accurate enough to realize such a specific hazard study. Finally, we conclude on the

112 importance of forearc crustal faults as potential major tsunami sources in subduction

113 zones.

114

2. Geological settings

116

117   Oceanic lithosphere of the North and South American plates is slowly subducting

118 beneath the Caribbean plate at a convergence rate of ~20mm·yr^{-1} (Figure 1, DeMets et al.,

119 2000; Philippon and Corti, 2016). The convex trench geometry results in along strike

120 variations of obliquity, increasing northward from Guadeloupe. Along the arc, oblique

121 subduction is accommodated by trench-parallel left-lateral strike slip faults such as the

122 Harvers-Montserrat-Bouillante / Les Saintes corridor (located within the volcanic arc),

123 the Bunce fault (located along the crustal buttress), and a series of trench-perpendicular

124 grabens forming a sinistral horsetail (Feuillet et al., 2002; Feuillet et al., 2010; Ten Brink

125 et al., 2004; Boucard et al., 2021) (Figure 1, Figure 2A).

126   In the central Lesser Antilles, the Marie-Galante Basin (Guadeloupe Archipelago),

127 is located at the southern end of the aforementioned regional horsetail system and is

128 described as a conjugated normal fault system defining a trench perpendicular graben

129 (Figure 2 A; Feuillet et al., 2001, 2011). This graben affects sediment deposits comprising

130 three regional mega-sequences: an Eocene(?) - Early Miocene MG-MS1 sequence, a mid-

Miocene – late Tortonian / early Messinian MG-MS2 sequence, and a Messinan to present MG-MS3 sequence (Bouysse et Mascle, 1994; De Min et al., 2015; Cornée et al., 2023). It shapes the Marie-Galante Basin (up to 1200 m water depth) and surroundings, Grande-Terre and Marie-Galante Islands, respectively (Figure 1). The northern boundary of the Marie-Galante Basin is the east trending, south dipping Gosier fault that runs primarily onshore along the southern coast of Grande-Terre (Garrabé and Andreieff, 1988; Figure 2A). The southern boundary of the basin consists of the N100° trending, ~50 km-long, north dipping Morne Piton fault, which crosscuts the northern edge of Marie-Galante Island (Bouysse et al., 1993) and extends offshore on both sides of the island (Feuillet et al., 2002, 2004).

The Morne Piton fault system consists of five main 5-15 km-long segments trending N90°E ± 30° separated by N140°E shorter right-lateral relays (Figure 2). The fault scarp is exposed at Anse Piton, eastern coast of Marie-Galante, and shows dip-slip striations (Feuillet et al., 2002). Onshore Marie-Galante, the fault offsets the Pliocene to middle Pleistocene platform by ∼60 m. It also crosscuts a series of 3 uplifted late-mid to late Pleistocene terraces along the eastern side of the island. Feuillet et al. (2004) calculated a 5 km dislocation depth and a 70 to 80°N fault dip to model the observed flexure of the footwall. Considering that the Marie-Galante Plateau is a flat abandoned 330 Ka old marine terrace, these authors estimate the average slip rate of the Morne Piton at about 0.5±0.2 mm·yr^{-1} since 330 Ka. Regarding the uplifted terraces they estimated a maximum earthquake moment magnitude (M_w) ranging from 5.8 up to 6.5 with a 400-1000 to 1400-3300 years of recurrence time, respectively (250 km^2 of estimated ruptured area). Moreover, it was later demonstrated that this plateau emerged between 1.77 and 1.07 Ma (magnetostratigraphic Chron 1R2r: Cornée et al., 2012; Münch et al., 2014; De Min et al., 2015; Léticée et al., 2019; Cornée et al., 2021). Note that considering an older age for the Plateau emergence would drastically lower the slip rate estimate and increase the recurrence time calculated by Feuillet et al. (2001).

3. Historical seismicity

Upper plate seismicity in the Marie-Galante Basin provided by (i) CDSA Seismic database (Antilles Seismological Data Center - Bengoubou-Valerius et al. (2008); Massin et al.(2021)), (ii) IRIS database (IRIS https://www.isc.ac.uk (Figure 2B) and (iii) the

deployment of Ocean Bottom Seismometers (OBS) (Ruiz et al., 2013; Bie et al., 2020) shows a widely distributed pattern of moderate magnitude earthquakes ($M_w \leq 5.3$), with the exception of the 2004 seismic cluster in Les Saintes. Wide Angle Seismic (WAS) profiles together with earthquakes data indicate a seismogenic crustal thickness limited to the first 15-20 km west of Marie-Galante suggesting a brittle-ductile transition at this depth (Kopp et al., 2011; Ruiz et al., 2013; Gonzalez et al., 2017; Padron et al., 2021). Among the very few focal mechanisms available in the Marie-Galante Basin (Gonzalez et al., 2017), the 25 February 2014 M_w 3.8 earthquake occurred beneath the southern Grande-Terre platform and shows pure normal motion along sub-E-W trending nodal planes (Gonzalez et al. 2017, Event n°9, hypocentral location accuracy of ca. 5 km; Figure 2C). The location, depth and nodal plane characteristics (57° dip and N102°E) of the earthquake indicate that the event may correspond to a rupture along the Gosier fault system, which is the only major fault system in the vicinity of the hypocentral location able to trigger such magnitude earthquake. Feuillet (2000) provided more than 20 focal mechanisms for earthquakes showing local magnitude 2<Ml<3.7 and one Ms=5.6 earthquake, located in and around the Marie-Galante Graben. All focal mechanisms show nearly pure normal motion along sub-E-W trending nodal planes, consistent with kinematics indicators observed along the Gosier and Morne Piton faults. This tectonic pattern is confirmed by GNSS velocities which indicate that a small trench-parallel extension is accommodated in the upper plate forearc (van Rijsingen et al., 2021).

Two historical earthquakes are reported along these two fault systems: (i) the 16 May 1851 earthquake with a maximum intensity of VII recorded in the southeastern part of Basse-Terre, is attributed to the Morne Piton fault with an estimated moment magnitude M_w=6.0 (Feuillet et al., 2011; and (ii) the 29 April 1897 earthquake with a maximum intensity of VIII recorded in the Pointe-à-Pitre area being either attributed to the Gosier Fault system with an estimated moment magnitude M_w=5.5, or to the Montserrat fault zone, with an estimated moment magnitude M_w=6.5 (Bernard and Lambert, 1988; Feuillet et al., 2011). Overall, at the latitude of Guadeloupe, regional earthquake data suggests that normal fault systems are active with an ability to generate earthquakes of moment magnitude M_w 6 and above. This magnitude range is potentially able to trigger tsunami according to tsunami catalogues (as explained, for example, in Roger et al., 2019).

197

4. Historical tsunami

199

Southwest of the Marie-Galante Basin, the 2004 M_w 6.3 earthquake (Bazin et al., 2010; Feuillet et al., 2011) showed that upper plate crustal faults can generate strong earthquakes and tsunamis. The main shock occurred along the NNW-SSE trending, *ca.* 40 km-long arc-parallel Les Saintes Fault System (Feuillet et al., 2011; Leclerc et al., 2016). The recurrence of such a rupture is estimated to be a few hundred years or more (Escartín et al., 2016; Escartín et al., 2018; Feuillet et al., 2011; Le Friant et al., 2008). Focal mechanisms of the main shock as well as five aftershocks provided an overall pure normal motion along NNW-SSE nodal planes (Figure 2D). Source models from Salichon et al. (2009), Bazin et al. (2010), and Feuillet et al. (2011), well constrained by the long duration of the aftershock sequence, proposed a main source localized along the N135°E trending, 50°E dipping Roseau Fault (westernmost fault of Les Saintes fault system) with a 30 km-long and 21 km-downdip width fault plane. Aftershock seismicity reactivated several nearby conjugate faults with a maximum seismic depth at *ca.* 15 km. The main rupture occurred at two asperities located 8 km below the surface with a maximum slip of 1.8 m, and propagated to the surface triggering a coseismic offset of the seafloor of 0.3-0.6 m along a *ca*. 10 km-long segment. Escartín et al. (2016) investigated the fault scarp by the mean of HR bathymetry highlighting a 3 km-long, up to 0.9 m-high scarp, but concluded that part of the observed slip may be post-seismic. The Les Saintes earthquake generated up to 2 m-high tsunami waves at the coast and a maximum horizontal run-up of 42 m in some bays of Les Saintes (Zahibo et al., 2005; Le Friant et al., 2008; Cordrie et al., 2020). However, tsunami models using fault parameters based on seismological data resulted in an underestimation of the tsunami wave amplitude and run-up (Le Friant et al., 2008). Cordrie et al. (2020) consider that their best fit models require greater slip on the fault plane and a greater magnitude for the earthquake than those given by the seismological data in order to accurately reproduce the observed tsunami, suggesting that the observed scarp is the surface expression of co-seismic slip (source parameters: M_w =6.4-6.5 – fault plane 15x15 km – Strike N325°E – Dip 55°E – rake ca.90° - slip=2.5-3.5 m).

Over the last ~500 years of historical written archives in the Lesser Antilles, a few dozen confirmed tsunamis from different origins (local, regional or far-field sources

including earthquakes, landslides, volcanic eruptions or combinations of them) have been reported. Starting with the 16 April 1690 Ms~8.0 Barbados earthquake (which presumably triggered the first reported tsunami in the Lesser Antilles), it includes the widely studied 1 November 1755 Lisbon transoceanic tsunami (*e.g.,* Gutscher et al., 2006, Accary and Roger, 2010; Roger et al., 2010, 2011, Martínez -Loriente et al., 2021) and the 18 November 1867 Virgin Islands tsunami (*e.g*., Zahibo et al., 2003, 2005; Barkan and ten Brink, 2004). Landslide sources and/or pyroclastic flows, are also known for their tsunamigenic potential. There are more and more studies led to assess the hazard associated to these "silent tsunamis" (e.g., Roger et al., 2024). In the Caribbean Region, a few tsunamis triggered by landslides and/or pyroclastic flows have been reported in catalogues of events (e.g., O'loughlin and Lander, 2003; Accary and Roger, 2010), bathymetric surveys helped to identified large submarine landslide scars and deposits (e.g., Deplus et al., 2001; Le Friant et al., 2009, 2019) and a few studies have highlighted the capacity of these landslides to trigger large tsunamis (e.g., Smith and Shepherd, 1996; Teeuw et al., 2009; Leslie and Mann, 2016).

On the basis of an extensive literature review, including cross-checking of information, we conclude that only four tsunamis reported in Guadeloupe are likely of upper crustal seismic origin (Mallet, 1853, 1854, 1855; Lander, 1997; Zahibo and Pelinovsky, 2001; Lander et al., 2003; O'Loughlin and Lander, 2003; Zahibo et al., 2003; Accary and Roger, 2010; Nikolkina et al., 2010; Roger et al., 2013; online databases: NGDC/WDS, 2023; TL/ICMMG, 2023). These tsunamis have been observed or recorded following earthquakes occurring on regional faults (indicated magnitude and epicenter coordinates are from the USGS online earthquakes catalogue: https://www.usgs.gov/programs/earthquake-hazards): the M_w~8.0-8.5 earthquake on 8 February 1843 (NE of Guadeloupe, 16.73°N, 61.17°W) and the M_w 7.2 earthquake on 25 December 1969 (SE of Guadeloupe, 15.648°N, 59.694°W) are arguably attributed either to a rupture along the megathrust or to upper plate faulting ; the M_w 6.5 earthquake on 16 March 1985 (along the Harvers-Montserrat-Bouillante fault system between Montserrat and Nevis, north of Basse-Terre, 17.013°N, 62.448°W); and the M_w 6.3 earthquake on 21 November 2004 (Along the Les Saintes fault system, south of Basse-Terre, 15.679°N, 61.706°W)(Figure1). The largest earthquakes and tsunamis produced at subduction zones are expected to originate from rupture at the plate interface megathrust. However, historical records in the Lesser Antilles reveal that neither the

263   1843 M_w 7.5-8.5 nor the 1839 M_w 7.5-8.5 largest known earthquakes, although

264   destructive, have been followed by large tsunamis. However, Roger et al. (2013) showed

265   that the simulation of a Mw 8.5 1843-like megathrust earthquake would have produced

266   wave amplitudes of 5 m and more along the exposed coasts of Guadeloupe, which was not

267   reported in coeval documents. Feuillet et al. (2011) explain these two major earthquakes

268   by the great depth of the rupture along the megathrust that led to little seafloor

269   deformation. However, numerical simulation of worst-case scenarios for these two

270   ruptures along the megathrust evidence the possibilities of tsunami amplitudes up to 10

271   meters and above in some embayment (Roger et al., 2013; Colon-Useche et al., 2023. As

272   magnitude of crustal earthquakes is constrained by fault length, events occurring along

273   such crustal fault show a much smaller magnitude than megathrust earthquakes

274   consequently may form smaller seafloor offsets. Thus, most crustal earthquakes able to

275   trigger a tsunami do not produce significant sea surface deformation (only a few

276   centimeters amplitude in most cases) compared to subduction interface earthquakes.

277   Associated tsunamis are typically only visible on pressure gauge records (coastal gauges

278   or DART systems) after processing the data (*e.g.*, de-tiding, high-frequencies filtering,

279   etc.).

280

281   ### 3. Material and method

282

283   ### 3.1 Seismic lines

284   We present eight multichannel seismic (MCS) lines acquired during five

285   oceanographic campaigns (location on Figure 3A). These include high-resolution sparker

286   source seismic data from KaShallow 1 (Lebrun et al., 2008) and GEOBERYX03

287   oceanographic campaigns (Thinon and Bitri, 2003; Thinon et al., 2004 and 2010), mid

288   resolution GI airgun arrays seismic data from KaShallow 2 (Lebrun et al., 2008) and

289   Aguadomar (Deplus et al., 1998) cruises, and deep penetrating MCS data from the

290   Sismantilles 1 seismic experiment (Hirn, 2001) (Table 1).

291   Sismantilles 1 seismic data have been processed using CGG-Veritas Geovecteur®

292   software on board the R/V Nadir (Hirn et al., 2001). Processing includes band pass

293   filtering, internal and external mute, one step velocity analysis, NMO correction, stack,

294   predictive deconvolution and post-stack constant water-velocity time migration. The

295 KaShallow 1 and 2, Aguadomar and Geoberyx have been processed with Seismic Unix

296 software (Cohen and Stokwell, Center for Wave Phenomena, Colorado School of Mines).

297 The seismic processing includes band pass filtering, sea waves and spherical divergence

298 corrections, constant velocity or simple velocity gradient NMO correction and stack, and

299 constant water-velocity time migration. The reflection seismic lines are in millisecond

300 two-way-travel-time (mstwt). The velocities of the Wide Angle Seismic refraction (WAS)

301 profiles are in second two-way-travel-time (stwt).

302

303 *3.2 Bathymetry*

304 High-resolution bathymetric data were acquired during the KaShallow2

305 oceanographic campaign (Lebrun, 2009) using a Simrad EM300 multibeam echosounder.

306 We merged this data with Aguadomar (Deplus, 1999) and Sismantilles 2 (Laigle et al.,

307 2007) cruises Simrad EM12 Dual multibeam echosounder data available for the Marie-

308 Galante Basin. Vertical accuracy for these echosounders is plurimetric for typical water

309 depth found in the Marie-Galante Basin (<2000 m below mean sea-level, noted bsl

310 hereafter). Near-shore (0-200 m bsl) and onshore, very high-resolution bathymetric and

311 topographic data comes from the Litto3D database -

312 (https://www.geoportail.gouv.fr/donnees/litto3d last accessed on September 2024-

313 that includes airborne lidar survey and KaShallow-3 multibeam data acquired with a

314 RESON Seabat 8101 multibeam echosounder). The vertical accuracy for this second

315 dataset is better than one meter. We used the Caraibes software (ifremer) to process the

316 data and to produce a 25 m grid spacing Digital Elevation Model of the Marie-Galante

317 Basin and surrounding islands. Maps are produced using the open-access QGIS software

318 (https://www.qgis.org)

319

320 *3.3 Depth and time calibration of main geological boundaries.*

321 In order to measure offsets of unconformities on time-migrated seismic lines we

322 need to constrain the seismic velocities within the sediments. We used velocities from the

323 WAS profile (Kopp et al., 2011) in the south of Marie-Galante, that trends parallel to the

324 MCS line Agua116 (Cornée et al., 2023). The WAS velocities in the *ca*. 0.4 stwt (second

325 two way time) thick upper unit (MG-MS3 – Cornée et al., 2023) ranges between 2 and 2.5

326 km/s. The 3.25 km/s isochrones mimic the base of unit MG-MS2 and the 4.5 km/s

327 isochrones follow the acoustic basement below MG-MS1. Moreover, KaShallow 2 cruise

MCS data (Table 1) acquired with a 600 m long streamer allows us to determine the Normal Move Out velocities down to a depth of *ca*. 0.75 stwt in well-layered units such as shown on the seismic lines (Figure 3). Once converted into interval velocities using the "Hewitt Dix formula", we determine velocities in the upper unit from 1500 to 2750 m/s (Dix, 1955). Therefore, we use 1500 m/s in the water and 2000 m/s and 2500 m/s in the sediments to estimate (and bound) the depth of unconformities observed on time-migrated seismic lines (Table 2).

Offshore, several first order unconformities and sedimentary units were accurately dated using bio-stratigraphy analysis or radiochronology (Bouysse and Mascle, 1994; KaShallow Reasearch Program results: Münch et al., 2013; De Min et al., 2015; Cornée et al., 2023). The deepest dated unconformity, MG-SB2, which corresponds to the top of the MG-MS1 sequence, occurs on seismic lines east of Marie-Galante (thick orange line on Figure 5, lines AGUA97 – K09-09 – K09_45 - Sis7C). Along the seismic line Agua 97, the F8 fault scarp has been sampled at 514 m bsl just beneath the unconformity (KaShallow Cruise ROV dive, Figure 6). The samples, BMG2 and 4, yielded a Late Burdigalian/earliest Langhian age (Cornée et al., 2023). Thus, we propose 16 Ma ± 1Ma for the age of MG-SB2**.** Above, another regional unconformity MG-SB3 (Cornée et al., 2023) is identified east of Marie-Galante. It corresponds to the top of MG-MS2 sequence (thick purple line on the Figure 5 lines Agua97 – K09-09-08 – K09-45-44 – Sis7C). The age for this surface is bracketed between the overlaying Late Messinian GT carbonate platform (zones N18, 5.8-5.33 Ma –Cornée et al., 2023) and the underlying sedimentary unit dated Late Tortonian 8.57 ± 0.43 Ma (Ar-Ar, Münch et al., 2014). We thus consider 7 ± 1.5 Ma for the age of MG-SB3. West of Marie-Galante, the angular unconformity on line K09-90 North-West of Marie-Galante may corresponds to MG-SB3 (Figure 4). However, this reflector is too deep to be followed across the whole fault system. Within the uppermost sequence, MG-MS3, a remarkable unit boundary corresponding to a second order unconformity, can be easily correlated throughout the basin and onshore (red thick line on Figure 4). This unit boundary is Middle-Late Piazencian offshore and correlates onshore with the 3–2.9 Ma tectonically-induced erosional unconformity SB1 (see above; Cornée et al., 2023). Along the seismic line Ber03-30-31, the fault scarp immediately north of F3 and F4 has been sampled at 283 m bsl (KaShallow Cruise ROV dive, Figure 4). Samples, BC1 and BC2, yielded ages of 1.33 ± 0.23 Ma and 1.15. ± 0.12 Ma, respectively (Ar^{40}/Ar^{39} ages on plagioclases, Münch et al., 2013; 2014). These samples correspond to

361   a prominent seismic reflector within the upper unit of MG-MS3 sequence that can also be

362   easily correlated through all the seismic lines west of Marie-Galante. We thus retain an

363   average age of 1.29 ± 0.26 Ma for this seismic reflector (green line on Figure 4).

364

365   *3.4 Tsunami modeling*

366   In order to test the tsunamigenic potential of the fault system proposed herein, a

367   rupture scenarios has been elaborated and is presented hereafter.

368   Numerical simulations of tsunami generation and propagation were carried out

369   using COMCOT software (Cornell Multi-grid Coupled Tsunami: Liu et al., 1998; Wang,

370   2008; Wang and Power, 2011). COMCOT is widely used by the research community and

371   constantly tested notably through various real tsunami cases (e.g. Prasetya et al., 2011;

372   Gusman et al., 2019; Paris et al., 2021; Gusman et al., 2022; Roger et al., 2023). COMCOT

373   uses a modified staggered finite-difference scheme to solve linear and non-linear shallow

374   water equations in either spherical or Cartesian coordinate systems throughout a set of

375   nested grids allowing refinement of the bathymetric resolution in coastal areas. A two-

376   way nested grid configuration is implemented in the model to balance computational

377   efficiency and numerical accuracy (Wang 2008; Wang and Power 2011).

378   For this study, nesting has been used with two grid levels: the first grid is a 0.5

379   arcmin (~900 m) resolution grid of the Lesser Antilles (extent: 295°E, 302°E, 12°S, 18°S)

380   built from the global dataset GEBCO 2021 (GEBCO Compilation Group, 2021); the second

381   grid is a 3.75 arcsec (~115 m) spatial resolution grid focusing on the Guadeloupe

382   Archipelago and Dominica Island, including the location of the investigated Morne Piton

383   fault system as shown on Figure 1 (extent: 297.92°E, 300.22°E, 14.94°N, 16.717°N). This

384   second grid has been built from different datasets including the aforementioned

385   bathymetric data (§ 3.2). The highest resolution and the most recent data have been kept

386   first. Data gaps have been filled in with data from GEBCO (GEBCO Compilation Group,

387   2021) for offshore regions, and SRTM version 3.0 Global 1 arcsec data (NASA SRTM,

388   2013) for onshore regions. Continuity of the different datasets has been ensured using

389   kriging interpolation, which has proven to be one of the best methods to produce a well-

390   defined DEM, especially for smooth transitions between different resolution areas (e.g.

391   Bernardes et al., 2006; Arun, 2013; Ajvazi and Czimber, 2019). Note that Dominica was

392   included in the second grid in order to look at potential effects which could occur between

393 the different islands and also to assess the potential tsunami threat resulting from the
394 Morne Piton scenario on this neighboring island.

395 The initial sea-bottom displacement is calculated by COMCOT considering an
396 instantaneous rupture of the fault using the surface deformation model of Okada (1985),
397 and transmission of the deformation to the water column above is considered
398 instantaneous. Calculations of wave propagation have been done at mean sea level (MSL)
399 assuming a constant Manning's roughness coefficient of 0.011 for the seabed friction
400 (Wang et al., 2017). A higher friction coefficient leads to more energy dissipation of
401 tsunami waves, especially in shallow waters, slowing down their speed and reducing
402 their amplitude and impact (e.g. Dao and Tkalich, 2007). Considering the limited extent
403 of the interest zone (~250km x 200km), the rupture parameters (leading to a small
404 coseismic rupture) and the objective to look at potential localized effect as inter-islands
405 resonance, tsunami waves propagation time was set to 10 hours.

406
407 ## 4. RESULTS
408
409 ### 4.1 The Morne Piton fault system

410 The HR bathymetric data presented here above (section 3.2) allows to refine the
411 structural pattern of the Morne Piton fault system, especially offshore (Figures 3A - B).
412 The fault system splays eastward from the N120-N135°E trending Eastern Les Saintes
413 fault system located east-south-east of Basse-Terre to the N110-115°E trending Petite-
414 Terre fault system south-south-east of Grande-Terre (Figures 2 and 3). Thus, the fault
415 zone spreads over a 5-8 km wide and 50 km long zone with an average N100°E trend.

416 Morpho-bathymetric analysis allows us to identify surficial segments of the faults
417 that are reaching out the seafloor. The main fault scarp of the Morne Piton fault system is
418 the southernmost one, along which 11 fault segments of 1-10 km length can be identified
419 (Figure 3B). From west to east, the F1 segment trends N110° and then the fault steps left
420 along the N75°E trending F2 segment. A little farther east, the fault cuts the northern
421 Colombie Bank and the eastern Marie-Galante platform along closely spaced N90E
422 trending left or right stepping segments F3, F3', F4 and F5. Across the island, the F6
423 segment is a N130°N trending, 6 km long right step relay linking the F5 segment to the F7
424 N90°E trending one. Further east offshore Marie-Galante, two N80°E trending fault
425 segments, F8, 9, 10 and 11, arrange as overlap right steps. There, the fault scarp vanishes

426   in just a few kilometers. To the east of the line Sis7C, neither the sediments nor the

427   basement are affected by the north-dipping Morne Piton fault system (Figure 5). In

428   contrast, the seismic line Sis7C shows that the basement is southwardly downthrown by

429   the Petite-Terre fault system, along south dipping active and sealed faults to the north

430   and south of the Morne Piton fault system, respectively (Figure 5 location on Figure 3A) .

431   West of Marie-Galante, the Morne Piton fault system widens as closely spaced fault splays

432   trending N95°E to N100°E link the main fault scarp (F2, F3 and F4) to the antithetic

433   Goyave Fault system or die westward (Figure 4 location on Figure 3A). Eastward of the

434   F6 segment, some synthetic and a few antithetic faults splay northeastward and link with

435   the N110-115°E Petite-Terre Fault system.

436   The mean fault-scarp height west of Marie-Galante Island is ca. 100 m (Figure 3C).

437   Across Marie-Galante Island, the mean fault-scarp height reaches 200 m and controls the

438   staircase morphology of the island. East of the island, the Marie-Galante Canyon carved

439   the sedimentary units, clearing some of the fault planes increasing their apparent scarps

440   heights up to 400 m. To the east, the canyon meanders and cuts through the eastern tip

441   of the Morne Piton fault system (Figure 3 B and C). West of the island, at the vicinity of

442   the volcanic island of Basse-Terre, either recent deposits or the uppermost sedimentary

443   units seal most of the faults. These observations seem to indicate that the sedimentary

444   rate west of Marie-Galante and the erosional rate east of Marie-Galante (in the canyon)

445   exceed the vertical slip rate of the fault.

446   *4.2 Vertical slip rate estimates along the Morne Piton fault system*

447   To assess the average vertical slip rate along the Morne Piton fault system, we

448   estimated the fault offset of key dated reflectors across the entire length of the fault

449   system (Figures 4 and 5 – Table 2). West of Marie-Galante, the main offset of the 1.29 ±

450   0.26 Ma seismic reflector (green on Figure 4) increases from west to east (i.e., from the

451   westernmost extremity of the fault toward its center). Close to the eastern shore of Basse-

452   Terre Island (Figure 4, profile K09-96, and Table 1), the 1.29 Ma reflector is downthrown

453   by 110-115 m. Eastward, the reflector offset increases up to 230-257 m (Figure 4, line

454   K09-90, K08_24 and Table 2) and reaches a maximum of 300-322 m (Figure 4, lines

455   ber03_30-31, K08-59). Accordingly, the number of sealed structures across the fault

456   system decreases eastward (Figures 3 and 4). Thus, West of Marie-Galante, the Morne

Piton fault system accommodates a vertical slip rate increasing eastward up to 0.25 ± 0.08 mm·yr^{-1} over the last 1.29 ± 0.26 Ma (Table 2).

The 2.95 ± 0.05 Ma Unit Boundary (red line on figure 4) can only be correlated across the fault system along the K08-59 seismic line. Growth strata are observed in the deposits above the 2.95 Ma unit boundary (Figure 4, gray shadow on seismic lines), attesting for syn-sedimentary fault activity. This unit boundary offset reaches 550-620 m, leading to 0.20 ± 0.02 mm·yr^{-1} average vertical slip rate over the last 2.95 ± 0.05 Ma, i.e ca. 0,16 mm·yr^{-1} for the period 2,95 - 1,29Ma (Table 2). West of Marie-Galante Island, deeper reflectors cannot be identified and correlated across the fault system because of the limited seismic penetration.

However, east of Marie-Galante, the MG-SB2 sequence boundary dated to 16 ± 1Ma (orange in Figure 5 – see also Figure 5 in Cornée et al., 2023) is the only reflector that can be correlated on both sides of the fault system. In the hanging wall of the fault, the younger MG-SB3 7 ± 1.5Ma boundary (Purple in Figure 5) as well as a large part of the fault scarp are eroded by the Marie-Galante Canyon. The seismic line K09-09 (Figure 5) shows that the MG-SB3 unconformity records the Morne Piton fault inception: in the footwall of the fault, the stratigraphy of MG-MS2 sequence (comprised between MG-SB2 and MG-SB3) shows conformal deposits flexed upward while approaching the fault, whereas MG-MS3 deposits onlap onto MG-SB3 and present clear growth strata. We thus propose that the 16 ± 1 Ma sequence boundary is pre-tectonic and is tilted by the fault since its inception 7 ± 1.5 Ma ago (the age of MG-SB3; Figure 5, profile K09-45-45). Along the fault system East of Marie-Galante we calculated the strain rate from MG-SB2 offset since 7 ± 1Ma. From east to west the slip rate ranges from 0.067 ± 0.03 mm·yr^{-1} at the K09_44-45 seismic line, to 0.071 ± 0.02 mm·yr^{-1} along the K09_08-09 line. Seismic line Agua97 (Figure 5) presents the greatest offset of MG-SB2. However, this seismic line does not cross the southernmost F7 segment (the water depth is too shallow for ship navigation in the footwall compartment). We estimated the depth of MG-SB2 in the footwall compartment from the closest seismic line available that crosses the fault located 1 km east of the Agua97 line. We obtain an offset of 830-860 m leading to a maximum average vertical slip rate of 0.12 ± 0.03 mm·yr^{-1} since 7 ± 1.5 Ma, i.e ca. 0,07 mm·yr^{-1} for the period 7 - 2,95Ma (Table 2). Consequently, we propose that i) the vertical slip rate accommodated by the Morne Piton fault system increases progressively from each extremity of the fault toward its center, and ii) that the Morne Piton fault system is

490   characterized by an increasing slip rate from *ca.* 0.07 from its inception (*i.e.* 7 Ma ago) to

491   *ca.* 0.25 mm·yr^{-1} since 1.29 Ma (Table 2).

492   *4.3 Earthquakes parameters of Tsunami modeling*

493   ROV dive along the ber03_30-32 seismic line allowed observation of one of the main

494   morphologic scarps of the Morne Piton fault system across the F2 and F3' segments

495   (Figures 3 and 6). Across the upper plateau, between F2 and F3', we observed several

496   N90°E trending fractures parallel to the fault segments (Figure 6A). While descending

497   across the F3' scarp, the slope progressively steepens up from 45° at 157 m bsl to more

498   than 80° at 280 m bsl just a few meters above the toe of the scarp (Figure 6A, B and C).

499   This morphology suggests a ca. 128 m-high cumulative scarp for the F3' segment at that

500   location. The very last meter of the fault scarp above the toe of the slope presents a 100

501   cm-high polished vertical surface, partly altered, showing dip-slip striations indicating

502   pure normal motion along this fault segment (Figure 5D E and F). This exposed and partly

503   altered fault slip plane breaches the sea floor at high angle. Such a polished striated fault

504   scarp morphology is similar, although more altered, to the co-seismic fault scarp

505   observed at the toe of the Roseau Fault plane, after the Les Saintes earthquake (Escartín

506   et al., 2016). We conclude that this observation of the Morne Piton polished striated scarp

507   may correspond to one of the last co-seismic scarps formed during a major earthquake

508   (including possible post-seismic slip motion) along this fault. Alteration of the fault slip

509   plane suggests that the slip event occurred tens to several hundred years ago, *i.e.*, this

510   fault slip plane may correspond to a pre-instrumental earthquake (see discussion). From

511   this observed scarp we obtained a ratio of last event scarp over total scarp height (proxy

512   for the cumulative slip as determined on Figure 3) of ∼2,6%. With this ratio we calculated

513   an average scarp of ∼75 cm along the whole length of the fault and a maximum scarp of 2

514   m. Such an average scarp value corresponds to the surface expression of a magnitude M_w

515   ∼6.7 earthquake using the criteria of Wells and Coppersmith (1994), or even 7 according

516   to Thingbaijam et al. (2017). The same studies also provide a calculated maximum

517   displacement of ∼2m, consistent with the maximum observation along the scarp.

518   Moreover, the 45 km total length of the Morne Piton fault system measured from HR

519   bathymetry, together with the width of the fault given by the 10 to 15 km thick

520   seismogenic crust, lead to a rupture area ranging between ∼ 450 to 675 km^2 that would

521   generate a magnitude M_w ∼6.7 ± 0.1 earthquake corroborating the afore range of

522 magnitude deduced with other observations (e.g., M_w ranging between 6.6 and 6.8

523 according Wells and Coppersmith, (1994) and Leonard (2010) and around 7 according

524 to Thingbaijam et al., 2017). The rupture parameters for the different identified segments

525 of the fault shown on figure 3B are provided in Table 3. Geographic location of the center

526 of top of the fault plane and azimuth are provided based on our structural analysis

527 (section 4.1 and 4.3). Neither seismic lines which illustrate only a few hundred of meters

528 nor in-depth earthquake distributions (which is not enough resolved) allow to estimate

529 the dip of the Morne Piton fault system. Thus, after considering the influence of dip on

530 surface deformation which turns out to be negligible, we choose a mean dip of 75° for the

531 fault segments after Feuillet et al. (2004). The shape of the rupture area (along-strike

532 length x downdip width) and a slip of 1.89 m (maximum displacement estimated from

533 scarp heigh measurement) is implemented for each segment in order to fit with a total

534 fault surface of ca. 500 km², corresponding to a magnitude M_w 6.5 earthquake. Finally,

535 conformably to pure dip slip striations observed along the F3' segment (section 4.3) and

536 the F7 segment (Feuillet et al. 2002), we apply a rake of 90°, corresponding to a pure

537 normal faulting mechanism as observed by Feuillet et al. (2004) at Anse Piton and by the

538 ROV picture of the present study. Fault segments F8 and F9 are not straight, for the

539 purpose of modeling they have been divided into F8-F9 and F10-F11 (Figure 7).

540 Hereafter, we use these parameters to evaluate the potential tsunami hazard from the

541 Morne Piton fault for a worst-case plausible scenario rupturing all the segments

542 simultaneously.

543

544 *4.4 Plausible worst-case tsunami scenario and resulting hazard*

545 We present a worst-case plausible scenario, related to a rupture along all the

546 identified segments of the Morne Piton fault system as these 1 to 10 km-long segments

547 most probably root in-depth along a single fault zone (Feuillet et al., 2004). We rule out

548 the eventuality of testing a single 10 km-long segment of the Morne Piton fault system

549 rupture as it would generate a M_w<6.0 earthquake and would thus unlikely consist in a

550 tsunami source (e.g., Roger et al., 2019). Here, we use a plausible M_w 6.5 scenario, i.e a

551 magnitude slightly lower that the maximum magnitude M_w 6.7 deduced from the

552 morphological analysis, but close enough to the Les Saintes earthquakes magnitude as

553 both Les Saintes and Morne Piton fault systems share close morphological characteristics.

554 Our model would generate a tsunami with a significant energy/amplitude to accurately

highlight the potential consequences of tsunami waves' propagation and interaction with the peculiar shallow reliefs and major embayment located in and around the Marie-Galante Basin. Quantifying horizontal run-up at the coast and assessing tsunami risk following a rupture along this fault is out of the scope of the present study as such quantifications necessitate a better knowledge of the fault dynamic itself (return period of large events, etc.).

The initial surface elevation directly resulting from the Okada (1985)'s formulation is presented in Figure 7. Due to the high inclination of the fault planes (dip = 75°) dipping globally northward, a profile cut of the initial displacement is represented from the north to the south by a crest (positive elevation) and a trough (negative elevation). At t=0, the shallow water equations take over from this initial deformation and the propagation of the tsunami waves is calculated over the nested grids at adequate time steps. Figure 8 presents the state of the virtual water surface at six different times of the tsunami waves propagation from 1 to 16 minutes. The wave front initially parallel to the fault axes (t ≤ 1 min) is progressively influenced by the bathymetry within the very first minutes following the rupture, leading to an anisotropic propagation of the waves showing variability in space and time. In addition, the fact that the fault literally crosses Marie-Galante leads to the tsunami source being divided in two independent sources located on the west and east of this island: two tsunamis are therefore generated and called TsuW (on the west) and TsuE (on the east) hereafter. These two tsunamis propagate from their origin and wrap around Marie-Galante as shown at t=4 min of propagation. Then, between 4 and 9 min, the two tsunami fronts meet on the north and south of Marie-Galante. Meanwhile, the propagation of the TsuW waves meet the shallow waters of the Banc Colombie shoal (approx. coordinates: 15.98°N/-61.43°W; minimum water depth is about 35m), west of Marie-Galante: the waves' amplitude increases as they slow down and their interaction leads to a constructive interference resulting in a "new" tsunami source at the Banc Colombie shoal, mainly showing a negative wave propagating southward with some extensions toward Marie-Galante on the east and Les Saintes on the west.

Approaching the coasts, wave shoaling takes over, the reduction in water depth slowing down the waves and simultaneously increasing their amplitude. It leads to wave amplification as particularly shown along Marie-Galante north shore, the southeast coast of Basse-Terre and the south of Petite-Terre and eastern Grande-Terre (Figure 9).

588   After 10 hours of tsunami propagation, the maximum values of wave amplitude
589   reached on each point of the simulation domain are shown in Figure 9. The overall impact
590   of such an event is that the maximum wave amplitude is not going over 1.2 m, carefully
591   considering the 100 m resolution of the simulation domain: in fact, grid refinement at the
592   coast showing higher resolution would probably highlight higher wave amplitude in very
593   localized areas because of interaction with small underwater structures not represented
594   at this resolution, as well as non-linear effects. The patterns of those amplitudes indicate
595   that not only the fault region but also some coastal regions are exposed to tsunami waves
596   of 50 cm or more, which is above the usual beach and marine threat 30-cm threshold. It
597   is the case for the neighboring coasts of Marie-Galante, southeast Basse-Terre, south
598   Grande-Terre and the natural reserve of Petite-Terre. The southeast coast of Basse-Terre
599   is particularly exposed with wave amplitudes of more than 1 m (Figure 9a). A focus on
600   Les Saintes Archipelago highlights also wave amplitudes of more than 1 m, even between
601   the islands (Figure 9b). The northeast coast of Dominica is also affected but to a lesser
602   extent (maximum wave amplitudes of ~50 cm). Further high-resolution simulation,
603   including flow speed calculations, would help to correctly assess the related hazard on
604   this island. Virtual sea-level gauges have been added at different locations of grid 2
605   (Figure 9) in order to check if the model is stable and to look for possible resonance
606   (especially in Les Saintes Archipelago). The raw signal of seven VG (top figure 10)
607   highlights a clear decrease of the amplitude over the time on all stations. However, for
608   stations VG_1, VG_2 and VG_3, a low-frequency oscillation is clearly visible and lasts for
609   at least 10 hours. The amplitude spectrums on these three stations show that two peaks
610   with a period of ~8.5 min and 15 min respectively are present on the three signals at Les
611   Saintes, which is not the case for the stations out of the archipelago. Moreover, the high
612   amplitude negative wave southwardly propagating generated by the "new" tsunami
613   source at the Banc Colombie shoal, is shown by VG_1 on figure 10 with a peak to through
614   value of ~0.6 m. VG_2 and VG_3 also show it to a lesser extent a bit later.

615

5. Discussion

617

5.1. Upper plate fault tsunamigenic potential.

619   Les Saintes earthquake demonstrated that upper plate normal faults may generate
620    $M_w > 6$ tsunamigenic earthquakes in the Lesser Antilles. Les Saintes tsunami produced up

to 2 m high waves at the coast and 42 m distance run-up in a peculiar embayment (Zahibo et al. 2005). Such normal faults are prone to be tsunamigenic because their rupture is relatively shallow (compared to the megathrust), and their slip motion is favorable to large seafloor displacement. Together with their proximity to the islands, they are able to produce metric-high tsunami waves at the coast and tens to hundreds of meters of run up distances (depending on the topography). Therefore, upper plate crustal faults may represent a major potential tsunami hazard in the Lesser Antilles islands and particularly in the Guadeloupe Archipelago as pointed out by the Intergovernmental Oceanographic Commission held in Fort-de-France in 2019 (IOC-UNESCO, 2020). Similarly to Les Saintes Fault, we assume that the 50 km long Morne Piton fault poses a potential earthquake and tsunami hazard. The large scarp we observed at the toe of the Morne Piton fault suggests recent seismogenic rupture(s) along this structure, potentially tsunamigenic. However, this scarp might not be related to the 1851 historical event as the estimated magnitude M_w 5-5.5 for this earthquake appears too low to explain the observed scarp. Thus, a rupture of the fault along its whole length must not be excluded. Several other prominent onshore-offshore faults affect the seafloor and the topography of the archipelago and may represent both an earthquake and a tsunami hazard. However, the relationships between faults, earthquakes and tsunami is not clearly established as shown in the following examples.

Along the arc, the Harvers-Montserrat-Bouillante and Les Saintes fault systems are the most prominent tectonic features (Feuillet et al., 2010). To the south, Les Saintes Fault system dips east and defines a half-graben (Leclerc et al., 2016). The westernmost fault, the Roseau fault, ruptured during the 2004 M_w 6.3 earthquake and is most likely reloading stress and therefore quiet. Recurrence time for this earthquake has been estimated to be more than 1,000 years given the regional slow strain rate. However, the eastern normal faults of the system offset the seafloor over more than 30 km and present tilted blocks filled by fan shaped late Pleistocene deposits attesting for recent deformation. In the light of these observations, the eventuality of a tsunamigenic earthquake along these faults should be considered. To the North-West along the Harvers segment, a rupture occurred in 1985 with a M_w 6.5 earthquake showing strike-slip mechanisms. Beck et al., (2012) estimated a recurrence time of 6,500-7,000 years for such a M_w 6.5 event based on the vertical offset of coseismic deposits in hemipelagites imaged by very high-resolution seismic lines across the fault. In between these two

segments, the Montserrat-Bouillante segment is seismically quiet except if the 1897 (estimated M_w 7.0) earthquake occurred along this fault (Feuillet et al., 2011). However, no tsunami related to such a rupture has been reported. Seismic lines across the Montserrat-Bouillante fault (Feuillet et al., 2010; Legendre, 2018) reveal that the fault offsets the most recent units including the oldest reflector drilled during the IODP1395, that dates upper Gelasian *ca*. 1.8-2Ma (Le Friant et al. 2013). Given an offset of 0.3m stwt and a 2000-2500 m/s sediments velocity this provides a 0.15-0.2 mm·yr^{-1} slip rate. Thus, the Montserrrat-Bouillante segment should also be considered tsunamigenic (Figure 2).

South of Grande-Terre of Guadeloupe, the N90°E trending Gosier Fault system bounds 45 km of coastal area (Figure 2). The fault system offset the Mid-Pleistocene Grande-Terre plateau that culminates at +150 m from the offshore plateau that rests 15-20 mbsl (Münch et al., 2013). This suggests a long-term vertical slip rate ca. 0.10 mm·yr^{-1}. To the east of Grande-Terre, the fault crosscuts the MIS5e terrace attesting for Late Pleistocene activity of the fault. However, evaluation of paleo-seismicity along one eastern segment of the fault system by the means of trenches allowed the identification of recent surface ruptures, although superficial deposits remain undated (Terrier and Combes, 2002).

East of Guadeloupe, offshore, the Marie-Galante Basin is bounded to the east by the Karukera spur (Figure 2D), a 75 km long N-S trending submerged plateau that culminates 30 mbsl to the north offshore La Désirade Island, and gently dips southward down to *ca*. 1500 mbsl (De Min et al., 2015). The spur is bounded to the west by N150°E to N0°E trending, west dipping, and normal faults. These faults offset the middle Miocene sequence boundary (SB2) by up to *ca*. 2,700-2,900 m, leading to a long-term vertical slip rate of 0.16-0.18 mm·yr^{-1}. Recent deposits are clearly affected by tectonic activity (Seibert et al., 2020). Located far from the islands, the earthquake intensity felt onshore would be relatively low in the island, but a tsunami could propagate across the Marie-Galante Basin directly toward the coasts of the Lesser Antilles Arc islands.

5.2. Slip rate reassessment along the Morne Piton fault system

With this study, we evidence that the slip rate along the Morne Piton fault system increases through time with a maximum slip rate of 0.25 ±0,08 mm·yr^{-1} since the last 1.29 Ma. This slip rate is up to four times slower than previous estimates. Over the last 330 Ka, Feuillet et al. (2004) estimate a bulk slip rate along the Morne Piton fault as high as 1

mm·yr^{-1} over 330 – 125 Ka then decreasing to 0.3 mm·yr^{-1} since the last 125 Ka. This last value is close to the long-term slip rate obtained offshore in this study (Figure 11). These results suggest that the fault may present a fast slip rate during short periods of time (few 100 ka.) separated by long periods (million years) of low slip rate. The fast 1 mm·yr^{-1} rate was obtained considering that the terrace T2MG is offset by the fault by 159 m and dates MIS7e (249 Ka) and the upper-plateau of Marie-Galante corresponds to an abrasion surface from the MIS9e high stand (330 Ka) (Feuillet et al., 2004).

This latter statement can be reconsidered. The same *Agaricia sp.* limestone unit, and *Acropora sp.* limestone unit top the three islands, Grande-Terre – La Désirade – Marie Galante, suggesting they emerged synchronously (Feuillet et al., 2002; Cornée et al., 2012; Munch et al., 2013). In the 3 islands the youngest formation, *Acropora* unit, is not younger than 1.07 Ma and not older than 1.54Ma (Cornée et al., 2012; Münch et al., 2014). From the geological map of Bouysse et al. (1993), this unit rims Marie-Galante Island. In La Désirade, the Upper Plateau culminates at 276 m asl (above sea level), whereas the 330 Ka terrace is at 35 m asl (Lardeaux et al., 2013; Leticée et al., 2019). Consequently, the hypothesis stating that the plateau emerged 330 Ka ago can be ruled out in Marie-Galante. Based on the age of the latest deposit of the Marie-Galante Plateau that range between 1.54 and 1.07 Ma, a vertical slip rate of 0.15-0.22 mm·yr^{-1} can be calculated. This value is close to the ca. 0.25 mm·yr^{-1} obtained offshore for the slip rate along the Morne Piton fault system over the same period of time (Figure 11). As a consequence, it is not possible to conclude that the Morne Piton fault system has short periods of fast slip rate, but instead it probably increases through time, a reaching a maximum slip rate of 0.25 mm·yr^{-1} over the last million years. As a consequence, dividing by four the slip rate along the Morne Piton fault system is increasing the earthquake time recurrence along this fault system and thus the time recurrence of potential associated tsunami. Constraining the fault slip rate at the time scale of one or few seismic cycles may allow better estimates of seismic and tsunamigenic hazards of the Morne Piton fault system. This would require a better knowledge of in-depth fault geometry and identification of its active segments that could be obtained by the means of a microseismic survey (using Ocean Bottom Seismometers acquisition over 1-2 years or more). At present-day, BOTDR laser reflectometry is used to perform long-term monitoring of the Morne Piton fault using the network of submarine telecom fiber optic cables connecting Marie-Galante to the larger islands of Basse-Terre and Grande-Terre (Gutscher et al., 2023). It is to note that given

720 the slow strain rate and in the absence of rupture occurring along the fault during the

721 survey period, identifying slip rate across this fault system may require hundreds to

722 thousands of years. Moreover, very high-resolution seismic data across the fault in areas

723 of high sedimentation rates (*i.e.*, along the eastern coast of Basse-Terre Island) may

724 constrain the Holocene fault activity. Slip rate estimates can be obtained by coring and

725 dating of (i) the most recent deformed sediments as well as (ii) tsunami deposits in salt

726 marshes. Finally, such regional monitoring would also contribute to a survey of past and

727 potential landslides that may also be induced by earthquakes and which may locally

728 generate destructive waves.

729

730 *5.3. Bathymetric features control on tsunami wave propagation*

731 The aim of the tsunami simulation associated to the present study is not to

732 produce a precise hazard assessment for the islands of Guadeloupe, but rather to give an

733 overview of what could happen in terms of tsunami generation if all the identified

734 segments of the Morne Piton fault system ruptured together, and to identify a few gaps in

735 terms of scientific knowledge and operational activities. An accurate hazard assessment

736 study would require many rupture scenarii including combinations of the segments used

737 in this study, with variations of their parameters and sensitivity tests.

738 The main outcome of the simulation presented above lies in the fact that

739 submarine features play an important role on the tsunami waves behavior and amplitude.

740 Submarine canyons are known to focus the waves (e.g.: along the continental slope of the

741 middle American trench: Álvarez-Gómez et al., 2012; or at Nazarè Portugal: Martins et al.,

742 2010; do Carmo et al., 2022; Delpey et al., 2021). This behavior also occurs along the rime

743 of the island submarine plateau rising the wave amplitude as exemplified in front of the

744 most populated cities of south-eastern Grande-Terre (Figure 9). Shallow water plateaus

745 located around or between islands slow down the waves which leads to particular

746 propagation patterns like the wrapping around the relief (Figure 8). There, the wrapping

747 effect of the waves around Marie-Galante and the Colombie Bank results in two distinct

748 tsunami sources, i.e. a primary source at fault and a secondary one at the Colombie Bank

749 (Figure 8). Such a behavior, already shown in other regions, is able to considerably

750 amplify the impact of the tsunami on the coast opposite to the fault rupture (Chadha et

751 al., 2005; Chen et al., 2012). It is important to notice that the low resolution of the grid

752 used for the present simulations is a limiting factor in quantifying correctly the wave

amplitude along the shoreline. A higher resolution simulation grid would better reproduce the bathymetric features, especially in shallow waters, having a non-negligible impact on the waves' behavior and amplitude.

Our simulation also highlights interesting phenomena that would require further consideration in the framework of further tsunami hazard studies: wave oscillation, which could be attributed to a resonance effect, is clearly visible within the Les Saintes Archipelago, and potential wave trapping is also visible around those islands. If the second case is purely observation, the resonance between Les Saintes islands is clearly revealed by the single-sided Fourier amplitude spectrum (Figure 10) and the peak at ~15 min seems to be associated with the negative wave coming time after the initial wave front and related to the tsunami interaction with the Colombie Bank shoal. The records provided by the virtual gauges located beforehand within the archipelago (VG_1, VG_2 & VG_3) clearly shows a long-period oscillation of the signal which is not present on the gauges located outside of Les Saintes (VG_4, VG_5, VG_6 & VG_11). It shows how the frequency content of the incoming signal can affect the sea-level during many hours after the seismic rupture.

The numerical simulations performed by Cordrie et al. (2020) of the tsunami having followed the M_w 6.3 Les Saintes earthquake were able to match the witnesses' observations in Les Saintes (Zahibo et al., 2005). Despite the low resolution (100m) of the present simulation on Les Saintes, there are some similarities between the two studies of potential impacted zones, for example in Marigot or Grande Anse Bays. It also shows that other bays, like the ones located between Terre-de-Haut and Ilet à Cabrit, appear to be quite well protected and not exposed to relatively strong tsunami waves.

Finally, this study also highlights the exposed coastline of Dominica: on the north-northeast coast of the island (Figure 9), 50+ cm waves are simulated, showing that this island should integrate such a scenario of crustal fault rupture within its tsunami hazard assessment plan.

Conclusions

Thanks to HR bathymetry, reflection seismic data and rock/sediment samples, the analyses of the morphology and tectonic structures of the Marie Galante Basin located in the middle of the Guadeloupe Archipelago, allow to detail the structural pattern of this

786 region and to estimate a slip rate of *ca*. 0.1 mm·yr^{-1} increasing over the last million year
787 to 0.25 mm·yr^{-1}, along the Morne Piton fault system, , cross-cutting the basin. This
788 estimate divides the previously published estimations of the slip rate by four, and thus
789 increases the earthquake recurrence time associated to the Morne Piton fault system
790 from 1Ka to 4-5 Ka. We show that a seismic rupture associated to an earthquake showing
791 a moment magnitude M_w ~6.5 can occur along the Morne Piton fault system in case of the
792 rupture of the full length of the fault (all segments being considered connected at depth
793 in the present demonstration). Such an event would be tsunamigenic according to
794 numerical simulation results. The multi-segment tsunami modeling illustrates how
795 submarine morphological and structural features influences the propagation pattern of
796 the tsunami leading to constructing interferences and resonances, thus increasing the
797 tsunami threat on nearby islands, especially highlighting a resonance effect within the
798 Les Saintes Islands, not discussed so far (and potentially the explanation of the so-far
799 unreproduced run-up values of the 2004 tsunami). At a regional scale we evidenced that
800 several other regional faults such as Montserrat-Harvers-Bouillante Fault, Gosier Fault,
801 Karukera Spur Border Fault, may also be tsunamigenic. Indeed, although they have the
802 potential to produce relatively low magnitude (<7) earthquakes, their rupture could
803 occur at shallow depth and close to a highly populated coast. Therefore, scenarii with arc
804 and forearc crustal fault ruptures must be integrated within their tsunami hazard
805 assessment plan. For that, it is necessary to have a better knowledge of onshore-offshore
806 structural and seismogenic patterns of each individual major faults system as the regional
807 low strain rate leads to large recurrence time of tsunamigenic earthquakes (> 1,000
808 years), *i.e.* much greater than the historical record. In addition, these earthquakes could
809 also have the capacity to destabilize the sedimentary layers at the edge of plateaus and
810 canyons, triggering submarine mass failures, capable of triggering large but more
811 localized tsunamis.

812

813 ### *Competing interests*

814
815 The contact author has declared that none of the authors has any competing interests.
816

817 ### *Acknowledgements and data*

818

819   We are grateful to C. Deplus, A. Hirn (IPGP) and M. Laigle (GeoAzur) for providing

820   Aguadomar and Sismantilles seismic and bathymetry data and to I Thinon and P. Gennoc

821   (BRGM) for providing the Geoberyx seismic data. The Kashallow project was supported

822   by The French National Program DyETI from INSU-CNRS, by the European Interreg IIIB

823   "Caribbean Space" Fund engaged in Guadeloupe with the EFRD projects (op. 30-700) and

824   the Region Guadeloupe. Part of this study was funded by the New Zealand's Strategic

825   Science Investment Fund (SSIF). We warmly thank José A. Álvarez-Gómez and

826   anonymous reviewers for their constructive comments and the NHESS editor R. Omira

827   for hangling our manuscript.

828

Data availability and request

830

831   Litto3D data can be found at https://diffusion.shom.fr/loisir/litto3d-guad2016.html

832   French oceanographic fleet data can be obtain on demand via the Sismer online interface

833   following the cruise doi – Aguadomar: https://doi.org/10.17600/98010120; Sismantilles:

834   https://doi.org/10.17600/1080060 and https://doi.org/10.17600/7010020; Kashallow:

835   https://doi.org/10.17600/9020010;

836   Requests for the Geoberyx03 data must be addressed to the BRGM.

837   Some figures have been prepared using the Generic Mapping Tools Version 6 software

838   (Wessel et al., 2019).

839

840

Author Contribution

842   MP: Conceptualization; Investigation; Visualization; Data curation; Formal analysis; Methodology; Writing - original
843   draft; Writing - review & editing, JR: Conceptualization; Investigation; Data curation; Formal analysis; Methodology;
844   Writing - original draft; Writing - review & editing, JFL: Formal analysis; Investigation; Resources; Writing - review
845   & editing; IT: Formal analysis; Investigation; Resources; Writing - original draft; Writing - review & editing; OF:
846   Validation, Writing - review & editing; SM: Validation, Writing - review & editing; MAG: Investigation; Validation,
847   Writing - review & editing; LM: Resources; Writing - review & editing; JJC: Conceptualization; Investigation; Writing-
848   original drafr, Writing - review & editing.

849

850

References

Accary, F., & Roger, J., 2010. Tsunami catalog and vulnerability of Martinique (Lesser Antilles, France). Science of Tsunami Hazards, 29(3).

Ajvazi, B., & Czimber, K., 2019. A comparative analysis of different DEM interpolation methods in GIS: case study of Rahovec, Kosovo. Geodesy and cartography, 45(1), 43-48. https://doi.org/10.3846/gac.2019.7921

Álvarez-Gómez, J. A., Gutiérrez, O. Q. G., Aniel-Quiroga, Í., & González, M. (2012). Tsunamigenic potential of outer-rise normal faults at the Middle America trench in Central America. *Tectonophysics*, *574*, 133-143. https://doi.org/10.1016/j.tecto.2012.08.014

Arun, P.V., 2013. A comparative analysis of different DEM interpolation methods. The Egyptian, Journal of Remote Sensing and Space Science, 16(2), 133-139. https://doi.org/10.1016/j.ejrs.2013.09.001

Barkan, R. and Ten Brink, U., 2010. Tsunami simulations of the 1867 virgin island earthquake: Constraints on epicenter location and fault parameterstsunami simulations of the 1867 virgin island earthquake: Constraints on epicenter location. *Bulletin of the Seismological Society of America*, *100*(3), pp.995-1009. https://doi.org/10.1785/0120090211

Bazin, S., Feuillet, N., Duclos, C., Crawford, W., Nercessian, A., Bengoubou-Valerius, M., ... & Singh, S. C., 2010. The 2004–2005 Les Saintes (French West Indies) seismic aftershock sequence observed with ocean bottom seismometers. Tectonophysics, 489(1-4), 91-103. https://doi.org/10.1016/j.tecto.2010.04.005

Beck, C., Reyss, J.L., Leclerc, F., Moreno, E., Feuillet, N., Barrier, L., Beauducel, F., Boudon, G., Clément, V., Deplus, C. and Gallou, N., 2012. Identification of deep subaqueous co-seismic scarps through specific coeval sedimentation in Lesser Antilles: implication for seismic hazard. *Natural Hazards and Earth System Sciences*, *12*(5), pp.1755-1767. https://doi.org/10.5194/nhess-12-1755-2012

Bengoubou-Valerius, M., Bazin, S., Bertil, D., Beauducel, F., & Bosson, A. (2008). CDSA: a new seismological data center for the French Lesser Antilles. *Seismological Research Letters*, *79*(1), 90-102.

Bernard, P., & Lambert, J., 1988. Subduction and seismic hazard in the northern Lesser Antilles: Revision of the historical seismicity. Bulletin of the Seismological Society of America, 78(6), 1965-1983.

883 Bernardes, T., Gontijo, I., Andrade, H., Vieira, T.G.C., Alves, H.M.R., 2006. Digital Terrain Models
884   Derived from SRTM Data and Kriging. In: AbdulRaman A., Zlatanova S., Coors V. (eds)
885   Innovations in 3D Geo Information Systems. Lecture Notes in Geoinformation and
886   Cartography. Springer, Berlin, Heidelberg. https://doi.org/10.1007/978-3-540-36998-
887   1_51

888 Bie, L., Rietbrock, A., Hicks, S., Allen, R., Blundy, J., Clouard, V., Collier, J., Davidson, J., Garth, T.,
889   Goes, S., Harmon, N., Henstock; T., van Huenen, J., Kendall, M., Krüger, F., Lynch, L.,
890   Macpherson, C., Robertson, R., Tait, S., Wilknison, J. & Wilson, M., 2020. Along-arc
891   heterogeneity in local seismicity across the Lesser Antilles subduction zone from a dense
892   ocean-bottom seismometer network. Seismological Research Letters, 91(1), 237-247.
893   https://doi.org/10.1785/0220190147

894 Biggs, J., & Wright, T. J., 2020. How satellite InSAR has grown from opportunistic science to
895   routine monitoring over the last decade. Nature Communications, 11(1), 1-
896   4.https://doi.org/10.1038/s41467-020-17587-6

897 Bilek, S. L. (2010). Invited review paper: Seismicity along the South American subduction zone:
898   Review of large earthquakes, tsunamis, and subduction zone complexity. *Tectonophysics*,
899   *495*(1-2), 2-14. https://doi.org/10.1016/j.tecto.2009.02.037

900 Boucard, M., Marcaillou, B., Lebrun, J. F., Laurencin, M., Klingelhoefer, F., Laigle, M., Lallemand, S.,
901   Schenini, L., Graindorge, D., Cornee, J.J., Münch, P. & Philippon, M., 2021. Paleogene V-
902   shaped basins and Neogene subsidence of the Northern Lesser Antilles Forearc. Tectonics,
903   40(3), e2020TC006524. https://doi.org/10.1029/2020TC006524

904 Bouysse P., Garrabé F., Mauboussin T., Andreieff P., Battistini R., Carlier P., Hinschberger F. &
905   Rodet J. (1993). – Carte géologique du département de la Guadeloupe. Notice explicative:
906   Marie-Galante et îlets de la Petite-Terre, scale 1: 50, 000. – BRGM, Orléans, France.

907 Bouysse, P., Mascle, A. (1994). Sedimentary Basins and Petroleum Plays Around the French
908   Antilles. In: Mascle, A. (eds) Hydrocarbon and Petroleum Geology of France. Special
909   Publication of the European Association of Petroleum Geoscientists, vol 4. Springer, Berlin,
910   Heidelberg. https://doi.org/10.1007/978-3-642-78849-9_32.

911 Chadha, R. K., Latha, G., Yeh, H., Peterson, C., & Katada, T. (2005). The tsunami of the great
912   Sumatra earthquake of M 9.0 on 26 December 2004–Impact on the east coast of India.
913   *Current Science*, 1297-1301.

914 Chen, J. M., Liang, D., & Tang, H. (2012). Interaction between tsunami waves and isolated conical
915   islands. *Journal of Coastal Research*, *28*(5), 1270-1278.

916 Colon Useche, S., Clouard, V., Ioualalen, M., Audemard, F. and Monfret, T., 2023. Simulation of
917   tsunami inundation for the island of Martinique to nearby large earthquakes. *Bulletin of the*
918   *Seismological   Society   of   America*,   *113*(1),   pp.252-267.
919   https://doi.org/10.1785/0120220093

920 Cordrie, L., Gailler, A., Escartín, J., Feuillet, N., & Heinrich, P., 2020. Simulation of the 2004 tsunami
921   of Les Saintes in Guadeloupe (Lesser Antilles) using new source constraints. Natural
922   Hazards, 103(2), 2103-2129. https://doi.org/10.1007/s11069-020-04073-x

923 Cornée, J. J., Leticée, J. L., Münch, P., Quillevere, F., Lebrun, J. F., Moissette, P., Braga, C., Melinte-
924   Dobrinescu, M., De Min, L., Oudet, J. & Randrianasolo, A., 2012. Sedimentology,
925   palaeoenvironments and biostratigraphy of the Pliocene–Pleistocene carbonate platform
926   of Grande-Terre (Guadeloupe, Lesser Antilles forearc). Sedimentology, 59(5), 1426-1451.
927   https://doi.org/10.1111/j.1365-3091.2011.01311.x

928 Cornée, J. J., Münch, P., Philippon, M., Boudagher-Fadel, M., Quillévéré, F., Melinte-Dobrinescu, M.,
929   Lebrun, J.F., Meyer, S., Montheil, L., Lallemand, S., Marcailou, B., Laurencin, M., Legndre, L.,
930   Garrocq, C., Boucard, M., Beslier, M.O., Laigle, M., Schenini, L., Fabre, P.H. & Marivaux, L.,
931   2021. Lost islands in the northern Lesser Antilles: possible milestones in the Cenozoic
932   dispersal of terrestrial organisms between South-America and the Greater Antilles. Earth-
933   Science Reviews, 217, 103617. https://doi.org/10.1016/j.earscirev.2021.103617

934 Cornée, J.J., De Min, L., Lebrun, J.F., Quillévéré, F., Melinte-Dobrinescu, M., BouDagher-Fadel, M.,
935   Montheil, L. , Marcaillou, B., Thinon, I. and Philippon M., 2023. Paleogeographic evolution
936   and vertical motion of the central Lesser Antilles forearc since the Early Miocene: A
937   potential driver for land fauna dispersals between the americas. Marine and Petroleum
938   Geology, 152, 106264. https://doi.org/10.1016/j.marpetgeo.2023.106264

939 Dao, M. H., & Tkalich, P., 2007. Tsunami propagation modelling–a sensitivity study. Natural
940   Hazards and Earth System Sciences, 7(6), 741-754. https://doi.org/10.5194/nhess-7-741-
941   2007

942 Delpey, M., Lastiri, X., Abadie, S., Roeber, V., Maron, P., Liria, P., & Mader, J. (2021).
943   Characterization of the wave resource variability in the French Basque coastal area based
944   on   a   high-resolution   hindcast. *Renewable   Energy*,   *178*,   79-95.
945   https://doi.org/10.1016/j.renene.2021.05.167

946 DeMets, C., Jansma, P. E., Mattioli, G. S., Dixon, T. H., Farina, F., Bilham, R., Calais., E. & Mann, P.,
947   2000. GPS geodetic constraints on Caribbean-North America plate motion. Geophysical
948   Research Letters, 27(3), 437-440. https://doi.org/10.1029/1999GL005436

949 De Min, L., Lebrun, J. F., Cornée, J. J., Münch, P., Léticée, J. L., Quillévéré, F., Melinte-Dobrinescu, M.,
950   Randrianasolo, A., Marcaillou, B. & Zami, F., 2015. Tectonic and sedimentary architecture of
951   the Karukéra spur: A record of the Lesser Antilles fore-arc deformations since the Neogene.
952   Marine Geology, 363, 15-37. https://doi.org/10.1016/j.margeo.2015.02.007

953 Deplus C., 1998, AGUADOMAR cruise, RV L'Atalante, https://doi.org/10.17600/98010120

954 Deplus, C., Le Friant, A., Boudon, G., Komorowski, J.C., Villemant, B., Harford, C., Ségoufin, J. and
955   Cheminée, J.L., 2001. Submarine evidence for large-scale debris avalanches in the Lesser
956   Antilles Arc. Earth and Planetary Science Letters, 192(2), pp.145-157.

957 Dix, C.H., 1955. Seismic Velocities from Surface Measurements, Geophysics 20, no. 1, 68-86.
958   https://doi.org/10.1190/1.1438126

959 do Carmo, J. S. A. (2022). Dominant processes that amplify the swell towards the coast: the
960   Nazaré Canyon and the giant waves. *Research, Society and Development*, *11*(11),
961   e578111133804-e578111133804. https://doi.org/10.33448/rsd-v11i11.33804

962 Escartín, J., Leclerc, F., Olive, J. A., Mevel, C., Cannat, M., Petersen, S., Augustin, N., Feuillet, N.,
963   Deplus, C., Bezos, A., Bonnemains, D., Chavagnac, V., Choi, Y., Godard, M., Haaga, K., Hamelin,
964   C., Ildefonse, B., Jamieson, J.W., John, B.E., Leleu, T., MacLead, C.J., Massot-Campos, M.,
965   Nomikou, P., Paquet, M., Tominaga, M., Triebe, L., Campos, R., Gracias, N., Garcia, R.,
966   Andreani, M. & Vilaseca, G. (2016). First direct observation of coseismic slip and seafloor
967   rupture along a submarine normal fault and implications for fault slip history. *Earth and
968   Planetary Science Letters*, *450*, 96-107.https://doi.org/10.1016/j.epsl.2016.06.024

969 Escartín, J., Leclerc, F., Nathalie, F., Le Friant, A., Billant, J., Olive, J. A. L., Henri, M., Andreani, M.,
970   Arnaubec, A., Dano, A., Delorme, A., Deplus, C., Fournasson, M.L., Gini, C., Gracias, N.,
971   Hamelin, C., Istenic, K., Komorowski, J.C., Marchand C., Mevel, C., Onstad, S., Quidelleur, X. &
972   Garcia, R. (2018, December). Mapping the M_w 6. 3 2004 Les Saintes earthquake seafloor
973   rupture with deep-sea vehicles: Length, displacement, nature, and links between coseismic
974   deformation and erosion/sedimentation. In *AGU Fall Meeting Abstracts* (Vol. 2018, pp.
975   EP51D-1851).

Feuillet, N., 2000. Sismotectonique des Petites Antilles: Liaison entre activité sismique
    et volcanique (Doctoral dissertation, Paris 7).

Feuillet, N., Manighetti, I., & Tapponnier, P., 2001. Extension active perpendiculaire à la subduction dans l'arc des Petites Antilles (Guadeloupe, Antilles françaises). Comptes Rendus de l'Académie des Sciences-Series IIA-Earth and Planetary Science, 333(9), 583-590.

Feuillet, N., Manighetti, I., Tapponnier, P., & Jacques, E., 2002. Arc parallel extension and localization of volcanic complexes in Guadeloupe, Lesser Antilles. Journal of Geophysical Research: Solid Earth, 107(B12), ETG-3. https://doi.org/10.1029/2001JB000308

Feuillet, N., Tapponnier, P., Manighetti, I., Villemant, B., & King, G. C. P., 2004. Differential uplift and tilt of Pleistocene reef platforms and Quaternary slip rate on the Morne-Piton normal fault (Guadeloupe, French West Indies). Journal of Geophysical Research: Solid Earth, 109(B2). https://doi.org/10.1029/2003JB002496

Feuillet, N., Leclerc, F., Tapponnier, P., Beauducel, F., Boudon, G., Le Friant, A., Deplus, C., Lebrun, J.F., Nercessian, A., Saurel, J.M. & Clément, V., 2010. Active faulting induced by slip partitioning in Montserrat and link with volcanic activity: New insights from the 2009 GWADASEIS marine cruise data. Geophysical Research Letters, 37(19). https://doi.org/10.1029/2010GL042556

Feuillet, N., Beauducel, F., & Tapponnier, P., 2011. Tectonic context of moderate to large historical earthquakes in the Lesser Antilles and mechanical coupling with volcanoes. Journal of Geophysical Research: Solid Earth, 116(B10). https://doi.org/10.1029/2011JB008443

Fujita, M., Ishikawa, T., Mochizuki, M., Sato, M., Toyama, S. I., Katayama, M., Kawai, K., Mastumoto, Y., Yabuki, T., Asada, A. & Colombo, O. L., 2006. GPS/Acoustic seafloor geodetic observation: method of data analysis and its application. Earth, planets and space, 58(3), 265-275. https://doi.org/10.1186/BF03351923

Garrabe, F. and Andreieff P. 1988. Notice explicative de la feuille de la Grande-Terre- Carte géologique au 1/50000, Département de la Guadeloupe. BRGM.

GEBCO Compilation Group, 2021. GEBCO 2021 Grid (doi:10.5285/c6612cbe-50b3-0cff-e053-6c86abc09f8f)

Geli, L., Çağatay, N., Gasperini, L., Favali, P., Henry, P., & Çifçi, G., 2011. ESONET WP4-Demonstration Missions. MARMARA-DM final report. https://archimer.ifremer.fr/doc/00032/14324/

Goldfinger, C., Nelson, C. H., Morey, A. E., Johnson, J. E., Patton, J. R., Karabanov, E. B., Gutierrez-Pastor, J., Eriksson, A.T., Gracia, E., Dunhill, G., Enkin, R.J., Dallimore, A. & Vallier, T., 2012. Turbidite event history—Methods and implications for Holocene paleoseismicity of the

Cascadia subduction zone(No. 1661-F). US Geological Survey. https://doi.org/10.3133/pp1661F

Gonzalez, OL, Clouard, V., & Zahradnik, J., 2017. Moment tensor solutions along the central Lesser Antilles using regional broadband stations. Tectonophysics, 717, 214-225. https://doi.org/10.1016/j.tecto.2017.06.024

Gusman, A.R., Supendi, P., Nugraha, A.D., Power, W., Latief, H., Sunendar, H., Widiyantoro, S., Daryono, Wiyono, S.H., Hakim, A., Muhari, A., Wang, X., Burbidge, D., Palgunadi, K., Hamling, I., Daryono, M.R., 2019. Source model for the tsunami inside Palu Bay following the 2018 Palu earthquake, Indonesia. Geophysical Research Letters, 46, 8721-8730, https://doi.org/10.1029/2019GL082717.

Gusman, A.R., Roger, J., Power, W., Fry, B., Kaneko, Y., 2022. The 2021 Loyalty Islands earthquake (M_w7.7): Tsunami waveform inversion and implications for tsunami forecasting for New Zealand. Earth and Space Science, e2022EA002346, https://doi.org/10.1029/2022EA002346.

Gutscher, M. A., Roger, J., Baptista, M. A., Miranda, J. M., & Tinti, S. (2006). Source of the 1693 Catania earthquake and tsunami (southern Italy): New evidence from tsunami modeling of a locked subduction fault plane. *Geophysical Research Letters*, *33*(8).

Gutscher, M. A., Royer, J. Y., Graindorge, D., Murphy, S., Klingelhoefer, F., Aiken, C., Cattaneo, A., Barreca, G., Quetel, L., Riccobene, G., Petersen, F., Urlaub, M., Krastel, S., Gross, F., Kopp, H., Margheriti, L. Beranzoli, L., 2019. Fiber optic monitoring of active faults at the seafloor: I the FOCUS project. Photoniques, 32-37. https://doi.org/10.1051/photon/2019S432

Gutscher, M. A., Quetel, L., Cappelli, G., Quillin, J. G., Nativelle, C., Lebrun, J. F., & Philippon, M. (2023, May). Monitoring a commercially operating submarine telecom cable network in the Guadeloupe archipelago (Lesser Antilles) using Brillouin Optical Time Domain Reflectometry (BOTDR). In *EGU General Assembly Conference Abstracts* (pp. EGU-8569).

Hirata, K., Aoyagi, M., Mikada, H., Kawaguchi, K., Kaiho, Y., Iwase, R., Morita, S., Fujisawa, I., Sugioka, H., Mitsuzawa, K., Suyehiro, K. & Fujiwara, N., 2002. Real-time geophysical measurements on the deep seafloor using submarine cable in the southern Kurile subduction zone. IEEE Journal of Oceanic Engineering, 27(2), 170-181. https://doi.org/10.1109/JOE.2002.1002471

Hirn, A. (2001). SISMANTILLES 1 cruise report. *RV Nadir*.

IOC-UNESCO (2020). Experts Meeting on Sources of Tsunamis in the Lesser Antilles Fort-de-France, Martinique (France) 18–20 March 2019. Workshop Reports, (291), 55p. Open Access version : https://archimer.ifremer.fr/doc/00665/77736/

Kido, M., Fujimoto, H., Miura, S., Osada, Y., Tsuka, K., & Tabei, T., 2006. Seafloor displacement at Kumano-nada caused by the 2004 off Kii Peninsula earthquakes, detected through repeated GPS/Acoustic surveys. Earth, planets and space, 58(7), 911-915. https://doi.org/10.1186/BF03351996

Kopp, H., Weinzierl, W., Becel, A., Charvis, P., Evain, M., Flueh, E. R., Gailler, A., Galve, A., Hirn, A., Kandilarov, D., Klaeschen, D., Laigle, M., Papenberg, C., Planert, L. & Roux, E., 2011. Deep structure of the central Lesser Antilles Island Arc: relevance for the formation of continental crust. Earth and Planetary Science Letters, 304(1-2), 121-134. https://doi.org/10.1016/j.epsl.2011.01.024

Laigle M., Lebrun J.-F., Hirn A. 2007. SISMANTILLES 2 cruise, RV L'Atalante, https://doi.org/10.17600/7010020

Lander, J. F., & Whiteside, L. S., 1997. Caribbean tsunamis: an initial history. In Caribbean Tsunami Workshop, June (pp. 11-13).

Lander, J. F., Whiteside, L. S., & Lockridge, P. A., 2003. Two decades of global tsunamis. Science of Tsunami Hazards, 21(1), 3.

Lardeaux, J. M., Münch, P., Corsini, M., Cornée, J. J., Verati, C., Lebrun, J. F., Guillevere, F., Melinte-Dobrinescu, M., Leticee, J.L., Fietzke, J., Mazabraud, Y., Cordrey, F. & Randrianasolo, A., 2013. La Désirade island (Guadeloupe, French West Indies): a key target for deciphering the role of reactivated tectonic structures in Lesser Antilles arc building. Bulletin de la Société géologique de France, 184(1-2), 21-34. https://doi.org/10.2113/gssgfbull.184.1-2.21

Lebrun, J.-F., Cornée, J.-J., Münch, P., Guennoc, P., Thinon, I., Begot, J., Mazabraud, Y., Fournier, F., Feuillet, N., Randrianasolo, A., 2008. La Mission KaShallow 1 - N/O Antéa - 26 avril - 05 Mai - Sismique réflexion haute résolution dans le bassin de Marie-Galante - Avant-arc des Petites Antilles. Rapport de l'Université des Antilles et de la Guyane.

Leclerc, F., Feuillet, N., & Deplus, C., 2016. Interactions between active faulting, volcanism, and sedimentary processes at an island arc: Insights from Les Saintes channel, Lesser Antilles arc. Geochemistry, Geophysics, Geosystems, 17(7), 2781-2802. https://doi.org/10.1002/2016GC006337

1071 Le Friant, A., Heinrich, P., & Boudon, G., 2008. Field survey and numerical simulation of the 21
1072   November 2004 tsunami at Les Saintes (Lesser Antilles). Geophysical Research Letters,
1073   35(12). https://doi.org/10.1029/2008GL034051

1074 Le Friant, A., Boudon, G., Arnulf, A., & Robertson, R. E. 2009. Debris avalanche deposits offshore
1075   St. Vincent (West Indies): impact of flank-collapse events on the morphological evolution
1076   of the island. Journal of Volcanology and Geothermal Research, 179(1-2), 1-10.

1077 Le Friant, A., Ishizuka, O., Stroncik, N.A., and the Expedition 340 Scientists. 2013. *Proc. IODP,* 340:
1078   Tokyo (Integrated Ocean Drilling Program Management International, Inc.). doi:10.2204/
1079   iodp.proc.340.105.2013

1080 Le Friant, A., Lebas, E., Brunet, M., Lafuerza, S., Hornbach, M., Coussens, M., Watt, S., Cassidy, M.,
1081   Talling, P.J. and IODP 340 Expedition Science Party. 2019. Submarine landslides around
1082   volcanic islands: A review of what can be learned from the Lesser Antilles Arc. Submarine
1083   Landslides: Subaqueous Mass Transport Deposits from Outcrops to Seismic Profiles,
1084   pp.277-297.

1085 Legendre, L., Philippon, M., Münch, P., Leticee, J. L., Noury, M., Maincent, G., Cornee, J.J., Caravati,
1086   A., Lebrun, J.F. & Mazabraud, Y., 2018. Trench bending initiation: Upper plate strain pattern
1087   and volcanism. insights from the Lesser Antilles arc, St. Barthelemy island, French West
1088   Indies. Tectonics, 37(9), 2777-2797.

1089 Lehu, R., Lallemand, S., Ratzov, G., Babonneau, N., Hsu, S. K., Lin, A. T., & Dezileau, L., 2016. An
1090   attempt to reconstruct 2700 years of seismicity using deep-sea turbidites offshore eastern
1091   Taiwan. Tectonophysics, 692, 309-324. https://doi.org/10.1016/j.tecto.2016.04.030

1092 Leonard, M. (2010). Earthquake fault scaling: Self-consistent relating of rupture length, width,
1093   average displacement, and moment release. *Bulletin of the Seismological Society of*
1094   *America*, *100*(5A), 1971-1988.

1095 Leticée, J. L., Cornee, J. J., Münch, P., Fietzke, J., Philippon, M., Lebrun, J. F., De Min, L., &
1096   Randrianasolo, A., 2019. Decreasing uplift rates and Pleistocene marine terraces settlement
1097   in the central lesser Antilles fore-arc (La Désirade Island, 16° N). Quaternary International,
1098   508, 43-59. https://doi.org/10.1016/j.quaint.2018.10.030

1099 Leslie, S. C., & Mann, P. 2016. Giant submarine landslides on the Colombian margin and tsunami risk in
1100   the Caribbean Sea. Earth and Planetary Science Letters, 449, 382-394.

1101 Lewis, K. B. 1980. Quaternary sedimentation on the Hikurangi oblique-subduction and transform
1102   margin, New Zealand. *Sedimentation in oblique-slip mobile zones*, 171-189.
1103   https://doi.org/10.1002/9781444303735.ch10

1104   Liu, P.L.F., Woo, S.B., Cho, Y.S., 1998. Computer programs for tsunami propagation and
1105   inundation. Ithaca (NY): Cornell University. Technical Report.

1106   Mallet, R., 1853. Catalogue of Recorded Earthquakes from 1606 B.C. to A.D. 1850, Part I,1606
1107   B.C. to 1755 A.D. Report of the 22nd Meeting of the British Association for the Advancement
1108   of Science, held in Belfast, Sept. 1852, John Murray, London, 177 pp.

1109   Mallet R. 1854. Catalogue of Recorded Earthquakes from 1606 B.C. to A.D. 1850, Part II, 1755 A.D.
1110   to 1784 A.D., Report of the 23Td meeting of the British Association for the Advancement of
1111   Science, held in Hull, Sept. 1853, John Murray, London, 118-212.

1112   Mallet R. 1855. Catalogue of Recorded Earthquakes from 1606 B.C. to A.D. 1850, Part III, 1784
1113   A.D. to 1842 A.D., Report of the 24" Meeting of the British Association for the Advancement
1114   of Science, John Murray, London, 326 pp.

1115   Martins, I., Vitorino, J., & Almeida, S. (2010, May). The Nazare Canyon observatory (W Portugal)
1116   real-time monitoring of a large submarine canyon. In *OCEANS'10 IEEE SYDNEY* (pp. 1-7).
1117   IEEE.

1118   Martínez-Loriente, S., Sallarès, V., & Gràcia, E., 2021. The Horseshoe Abyssal plain Thrust could
1119   be the source of the 1755 Lisbon earthquake and tsunami. *Communications earth &*
1120   *environment*, *2*(1), 145. https://doi.org/10.1038/s43247-021-00216-5

1121   Massin, F., Clouard, V., Vorobieva, I., Beauducel, F., Saurel, J. M., Satriano, C., Bouin, M. P., & Bertil,
1122   D. (2021). Automatic picking and probabilistic location for earthquake assessment in the
1123   lesser antilles subduction zone (1972-2012). In Comptes Rendus - Geoscience (Vol. 353,
1124   Issue   S1).   Academie   des   sciences.   https://doi.org/10.5802/crgeos.81.
1125   https://doi.org/10.5802/crgeos.81

1126   McCalpin, J.P. 1996. (Ed.), Paleoseismology, Academic Press, London, p. 583

1127   Münch, P., Lebrun, J. F., Cornée, J. J., Thinon, I., Guennoc, P., Marcaillou, B. J., Begot, J., Bertrand, G.,
1128   Bes De Berc, S., Biscarrat, K., Claud, C., De Min, L., Fournier, F., Gailler, L., Grandorge, D.,
1129   Leticee, J.L., Marie, L., Mazabraud, Y., Melinte-Dobrinescu, M., Moisette, P., Quilevere, F.,
1130   Verati, C. & Randrianasolo, A., 2013. Pliocene to Pleistocene carbonate systems of the
1131   Guadeloupe archipelago, French Lesser Antilles: a land and sea study (the KaShallow
1132   project).   Bulletin   de   la   Société   géologique   de   France,   184(1-2),   99-110.
1133   https://doi.org/10.2113/gssgfbull.184.1-2.99

1134   Münch, P., Cornee, J. J., Lebrun, J. F., Quillevere, F., Verati, C., Melinte-Dobrinescu, M., Demory, B.,
1135   Smith, F., Jourdan, J.M., Lardeaux, J.M., De Min, L., Leticee, J.L. & Randrianasolo, A., 2014.
1136   Pliocene to Pleistocene vertical movements in the forearc of the Lesser Antilles subduction:

insights from chronostratigraphy of shallow-water carbonate platforms (Guadeloupe archipelago). Journal of the Geological Society, 171(3), 329-341. https://doi.org/10.1144/jgs2013-005

NASA Shuttle Radar Topography Mission (SRTM)(2013). Shuttle Radar Topography Mission (SRTM) Global. Distributed by OpenTopography. https://doi.org/10.5069/G9445JDF. Accessed: 2022-12-07.

Nikolkina, I., Zahibo, N., & Pelinovsky, E., 2010. Tsunami in Guadeloupe (Caribbean Sea). The Open Oceanography Journal, 4(1). https://doi.org/10.2174/1874252101004010044

Okada, Y., 1985. Surface deformation due to shear and tensile faults in a half-space. Bulletin of the seismological society of America, 75(4), 1135-1154. https://doi.org/10.1785/BSSA0750041135

O'loughlin, K. F., & Lander, J. F., 2003. Caribbean tsunamis: a 500-year history from 1498-1998 (Vol. 20). Springer Science & Business Media.

Padron, C., Klingelhoefer, F., Marcaillou, B., Lebrun, J. F., Lallemand, S., Garrocq, C., Laigle, M., Roest, W.R., Beslier, M.O., Schenini, L., Graindorge, D., Gay, A., Audemard, F., Munch., P. & GARANTI Cruise Team., 2021. Deep structure of the Grenada Basin from wide-angle seismic, bathymetric and gravity data. Journal of Geophysical Research: Solid Earth, 126(2), e2020JB020472. https://doi.org/10.1029/2020JB020472

Paris, R., Sabatier, P., Biguenet, M., Bougouin, A., André, G., Roger, J., 2021. A tsunami deposit at Anse Meunier, Martinique Island: evidence of the 1755 CE Lisbon tsunami and implication for hazard assessment. Marine Geology, 439, 106561, https://doi.org/10.1016/j.margeo.2021.106561.

Petersen, F., Kopp, H., Lange, D., Hannemann, K., & Urlaub, M., 2019. Measuring tectonic seafloor deformation and strain-build up with acoustic direct-path ranging. Journal of Geodynamics, 124, 14-24. https://doi.org/10.1016/j.jog.2019.01.002

Philippon, M., & Corti, G., 2016. Obliquity along plate boundaries. Tectonophysics, 693, 171-182. https://doi.org/10.1016/j.tecto.2016.05.033

Prasetya, G., Beavan, J., Wang, X., Reyners, M., Power, W., Wilson, K., Lukovic, B., 2011. Evaluation of the 15 July 2009 Fjorland, New Zealand tsunami in the source region. Pure and Applied Geophysics, 168, 1973-1987, https://doi.org/10.1007/s00024-011-0282-6.

Roger, J., Allgeyer, S., Hébert, H., Baptista, M. A., Loevenbruck, A., & Schindelé, F., 2010. The 1755 Lisbon tsunami in Guadeloupe Archipelago: source sensitivity and investigation of

1169   resonance effects. The Open Oceanography Journal, 4(1).
1170   https://doi.org/10.2174/1874252101004010058

1171 Roger, J., Baptista, M. A., Sahal, A., Accary, F., Allgeyer, S., & Hébert, H., 2011. The transoceanic
1172   1755 Lisbon tsunami in Martinique. Pure and Applied Geophysics, 168(6), 1015-1031.
1173   https://doi.org/10.1007/s00024-010-0216-8

1174 Roger, J., Dudon, B., & Zahibo, N., 2013. Tsunami hazard assessment of Guadeloupe Island (FWI)
1175   related to a megathrust rupture on the Lesser Antilles subduction interface. Natural
1176   Hazards and Earth System Sciences, 13(5), 1169-1183. https://doi.org/10.5194/nhess-13-
1177   1169-2013

1178 Roger, J., Pelletier, B., & Aucan, J. (2019). Update of the tsunami catalogue of New Caledonia using
1179   a decision table based on seismic data and marigraphic records. *Natural Hazards and Earth*
1180   *System Sciences*, *19*(7), 1471-1483. https://doi.org/10.5194/nhess-19-1471-2019

1181 Roger, J., Pelletier, B., Gusman, A., Power, W., Wang, X., Burbidge, D., & Duphil, M., 2023. Potential
1182   tsunami hazard of the southern Vanuatu Subduction Zone: tectonics, case study of the
1183   Matthew Island tsunami of 10 February 2021 and implication in regional hazard
1184   assessment. Natural Hazards and Earth System Sciences, 23(2), 393-414,
1185   https://doi.org/10.5194/nhess-23-393-2023.

1186 Roger, J.H., Bull, S., Watson, S.J., Mueller, C., Hillman, J.I., Wolter, A., Lamarche, G., Power, W., Lane,
1187   E., Woelz, S. and Davidson, S. (2024). A review of approaches for submarine landslide-
1188   tsunami hazard identification and assessment. Marine and Petroleum Geology,
1189   162(106729), https://doi.org/10.1016/j.marpetgeo.2024.106729.

1190 Ruiz, M., Galve, A., Monfret, T., Sapin, M., Charvis, P., Laigle, M., Evain, M., Hirn, A., Flueh, E., Gallart,
1191   K., Diaz, J., Lebrun, J.F. & Lebrun, J. F., 2013. Seismic activity offshore Martinique and
1192   Dominica islands (Central Lesser Antilles subduction zone) from temporary onshore and
1193   offshore seismic networks. *Tectonophysics*, *603*, 68-78.
1194   https://doi.org/10.1016/j.tecto.2011.08.006

1195 Salichon, J., Lemoine, A., Aochi, H., 2009. Validation of teleseismic inversion of the 2004 M_w6.3
1196   Les Saintes, Lesser Antilles, earthquake by 3D finite-difference forward modelling. Bull.
1197   Seismol. Soc. Am. 99, 3390–3401. https://doi.org/10.1785/0120080315

1198 Satake, K., & Tanioka, Y., 1999. Sources of tsunami and tsunamigenic earthquakes in subduction
1199   zones. Pure and Applied Geophysics, 154(3), 467-483.
1200   https://doi.org/10.1785/0120120306

1201   Seibert, C., Feuillet, N., Ratzov, G., Beck, C., & Cattaneo, A., 2020. Seafloor morphology and
1202   sediment transfer in the mixed carbonate-siliciclastic environment of the Lesser Antilles
1203   forearc along Barbuda to St. Lucia. Marine Geology, 428, 106242.
1204   https://doi.org/10.1016/j.margeo.2020.106242

1205   Smith, M. S., & Shepherd, J. B. (1996). Tsunami waves generated by volcanic landslides: an
1206   assessment of the hazard associated with Kick'em Jenny. Geological Society, London,
1207   Special Publications, 110(1), 115-123.

1208   Symithe, S. J., Calais, E., Haase, J. S., Freed, A. M., & Douilly, R., 2013. Coseismic slip distribution of
1209   the 2010 M 7.0 Haiti earthquake and resulting stress changes on regional faults. *Bulletin of*
1210   *the Seismological Society of America*, *103*(4), 2326-2343.
1211   https://doi.org/10.1785/0120120306

1212   ten Brink, U., Danforth, W., Polloni, C., Andrews, B., Llanes, P., Smith, S., Parker, E., and Uozumi, T.
1213   2004. New seafloor map of the Puerto Rico trench helps assess earthquake and tsunami
1214   hazards. Eos, Transactions American Geophysical Union 85: 349–360.
1215   doi:10.1029/2004EO370001.

1216   Terrier, M., Combes P. avec la collaboration de D. Carbon, B. Grellet, O. Sedan (2002) - FAILLES
1217   ACTIVES ET EVALUATION DE L'ALEA SISMIQUE : Prise en compte des failles actives dans
1218   l'aménagement du territoire aux Antilles (Martinique et Guadeloupe). Partie 1 :
1219   Identification des systèmes de failles actives dans l'archipel de la Guadeloupe et l'île de la
1220   Martinique. Rapport BRGM/RP-51258-FR. 118 pages. 30 figures. 8 tableaux. 4 annexes

1221   Teeuw, R., Rust, D., Solana, C., Dewdney, C., & Robertson, R. 2009. Large coastal landslides and
1222   tsunami hazard in the Caribbean. Eos, Transactions American Geophysical Union, 90(10),
1223   81-82.

1224   Thingbaijam, K.K.S., Mai, P.M. and Goda, K., 2017. New Empirical Earthquake Source-Scaling
1225   Laws. *Bulletin of the Seismological Society of America*, *107*(5), pp.2225-2246.
1226   https://doi.org/10.1785/0120170017

1227   Thinon, I, Bitri, A., 2003. GEOBERYX03 cruise, RV Beryx, Catalogue des campagnes à la mer
1228   (flotteoceanographique.fr)   ;browsed   on-line   on   Seadatanet   webportal
1229   (SISM_BGM_FI352003000010, https://cdi.seadatanet.org/);

1230   Thinon I., Bitri A., Guennoc P. & Truffert C. (2004). – Levés sismique et magnétique du plateau
1231   occidental de l'île de Basse-Terre, Guadeloupe (Campagne Geoberyx03). Apports à la
1232   compréhension du contexte structural du champ géothermique de Bouillante. – BRGM/RP-
1233   53152-FR, 77.

1234 Thinon, I., Guennoc, P., Bitri, A., Truffert C., 2010, Study of the Bouillante Bay (West Basse-Terre
1235   Island shelf): contribution of geophysical surveys to the understanding of the structural
1236   context of Guadeloupe (French West Indies - Lesser Antilles). Bull. Soc. Geol. Fr., 181, 51-
1237   65, http://doi.org/10.2113/gssgfbull.181.1.51

1238 TL/ICMMG (2023). Global Historical Tsunami Database. Institute of Computational Mathematics
1239   and Mathematical Geophysics SB RAS Tsunami Laboratory, Novosibirsk, Russia,
1240   http://tsun.sscc.ru/gtdb/default.aspx (last accessed on 1 February 2023).

1241 Tronin, A. A., 2009. Satellite remote sensing in seismology. A review. Remote Sensing, 2(1), 124-
1242   150. https://doi.org/10.3390/rs2010124

1243 van Rijsingen, E. M., Calais, E., Jolivet, R., de Chabalier, J. B., Jara, J., Symithe, S., ... & Ryan, G. A.,
1244   2021. Inferring interseismic coupling along the lesser antilles arc: A Bayesian approach.
1245   Journal of Geophysical Research: Solid Earth, 126(2), e2020JB020677.
1246   https://doi.org/10.1029/2020JB020677

1247 Wallace, T. C., Helmberger, D. V., & Ebel, J. E., 1981. A broadband study of the 13 August 1978
1248   Santa Barbara earthquake. *Bulletin of the Seismological Society of America*, *71*(6), 1701-
1249   1718. https://doi.org/10.1785/BSSA0710061701

1250 Wang, X., 2008. Numerical modelling of surface and internal waves over shallow and
1251   intermediate water [PhD thesis]. Ithaca (NY): Cornell University. 245 p.

1252 Wang, X., Power, W.L., 2011. COMCOT: a tsunami generation, propagation and run-up model.
1253   Lower Hutt (NZ): GNS Science. 121 p. (GNS Science report; 2011/43).

1254 Wang X, Lukovic B, Power WL, Mueller C., 2017. High-resolution inundation modelling with
1255   explicit buildings. Lower Hutt (NZ): GNS Science. 27 p. (GNS Science report 2017/13).
1256   https://doi.org/10.21420/G2RW2N.

1257 Wells, D. L., & Coppersmith, K. J., 1994. New empirical relationships among magnitude, rupture
1258   length, rupture width, rupture area, and surface displacement. Bulletin of the seismological
1259   Society of America, 84(4), 974-1002. https://doi.org/10.1785/BSSA0840040974

1260 Wessel, P., Luis, J.F., Uieda, L., Scharroo, R., Wobbe, F., Smith, W.H.F., Tian, D., 2019. The Generic
1261   Mapping Tools Version 6. Geochemistry, Geophysics, Geosystems, 20(11), 5556-5564,
1262   https://doi.org/10.1029/2019GC008515.

1263 Zahibo, N., Pelinovsky, E., Kurkin, A., & Kozelkov, A., 2003. Estimation of far-field tsunami
1264   potential for the Caribbean Coast based on numerical simulation. Science of Tsunami
1265   Hazards, 21(4), 202-222.

1266   Zahibo, N., Pelinovsky, E., Okal, E., Yalçiner, A., Kharif, C., Talipova, T., & Kozelkov, A., 2005. The

1267   earthquake and tsunami of November 21, 2004 at Les Saintes, Guadeloupe, Lesser Antilles.

1268   Science of Tsunami Hazards, 23(1), 25-39.

1269   Zhang, L., Baba, K., Liang, P., Shimizu, H., & Utada, H., 2014. The 2011 Tohoku Tsunami observed

1270   by an array of ocean bottom electromagnetometers. Geophysical Research Letters, 41(14),

1271   4937-4944. https://doi.org/10.1002/2014GL060850

1272
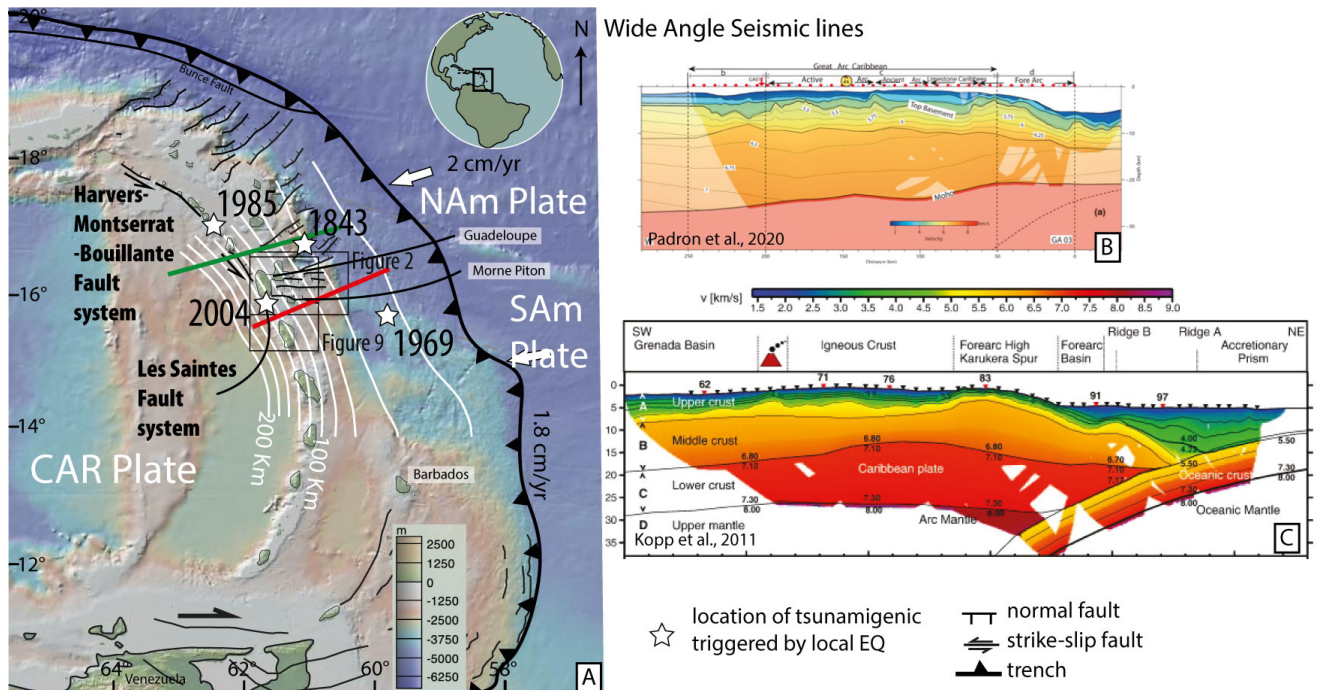
1275

*Figure 1: A: Synthetic tectonic map of the Lesser Antilles forearc. Structures after Feuillet et al.
(2002), Legendre et al. (2018), Boucard et al. (2021). Red and green thick lines indicate location of
the Wide Angle Seismic lines from B. Kopp et al. (2011) and C. Padron et al. (2021) respectively.
White Star: location of tsunamigenic earthquakes. Thick white contour lines: Slab depth isocontour
from Bie et al. (2020).*

1281
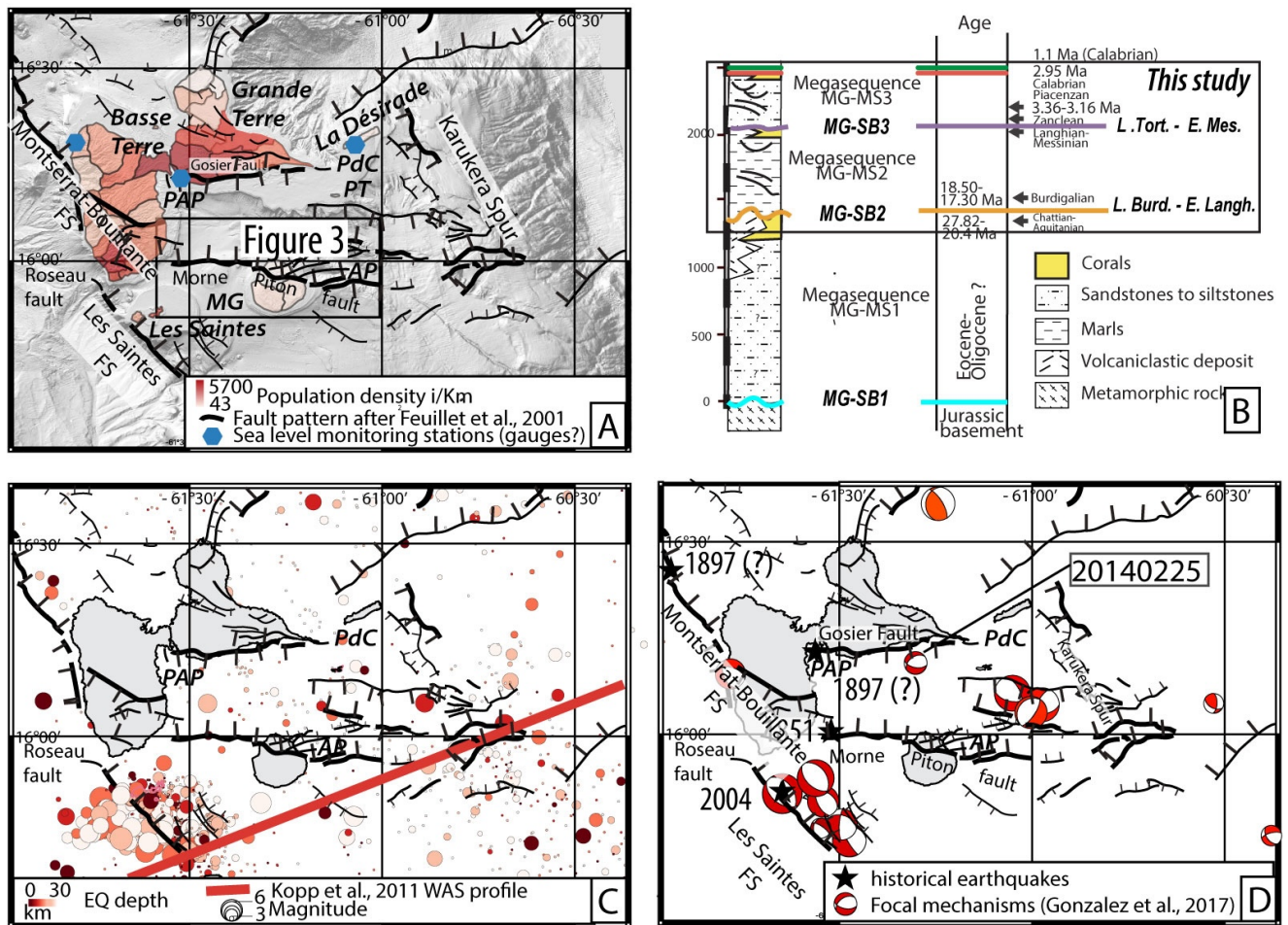
Figure 2. The Marie-Galante Basin A) structural pattern after Feuillet et al. (2002) and De Min et al. (2015) on the shaded-relief bathymetric map. blue hexagons : tide gauges http://refmar.shom.fr/fr/liste-maregraphes-data.shom.fr. Red colors scale: Guadeloupe population density per km2 after GEOFLA (https://www.data.gouv.fr/fr/datasets/geofla-r/). B) Sismostratigraphic scheme of the Marie-Galante basin modified after Cornée et al., 2023. C) Colored dots: Crustal seismicity (from IRIS seismic database 2023) for magnitude earthquakes (EQ) 3>M$_w$>6.5 and located from 0 to 30 km depth), red line locates the WAS line (Kopp et al., 2011). D) Focal mechanisms solutions are indicated by red beachballs after Gonzalez et al. (2017). The location of historical earthquakes is indicated by black stars (after: Feuillet et al., 2011). AP, PdC, PAP, PT stand for Anse Piton, Pointe des Chateaux, Pointe-à-Pitre and Petite Terre.
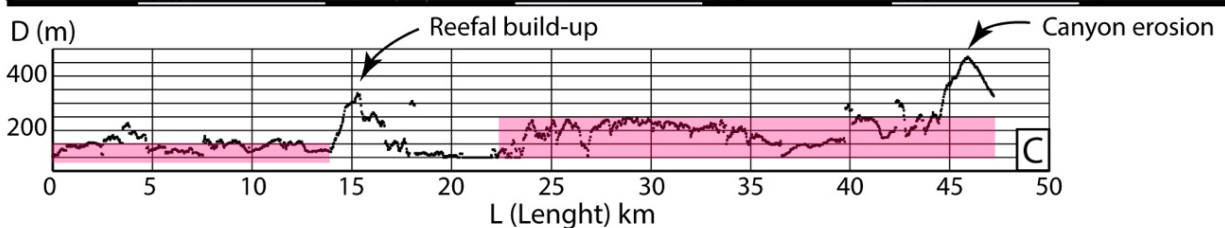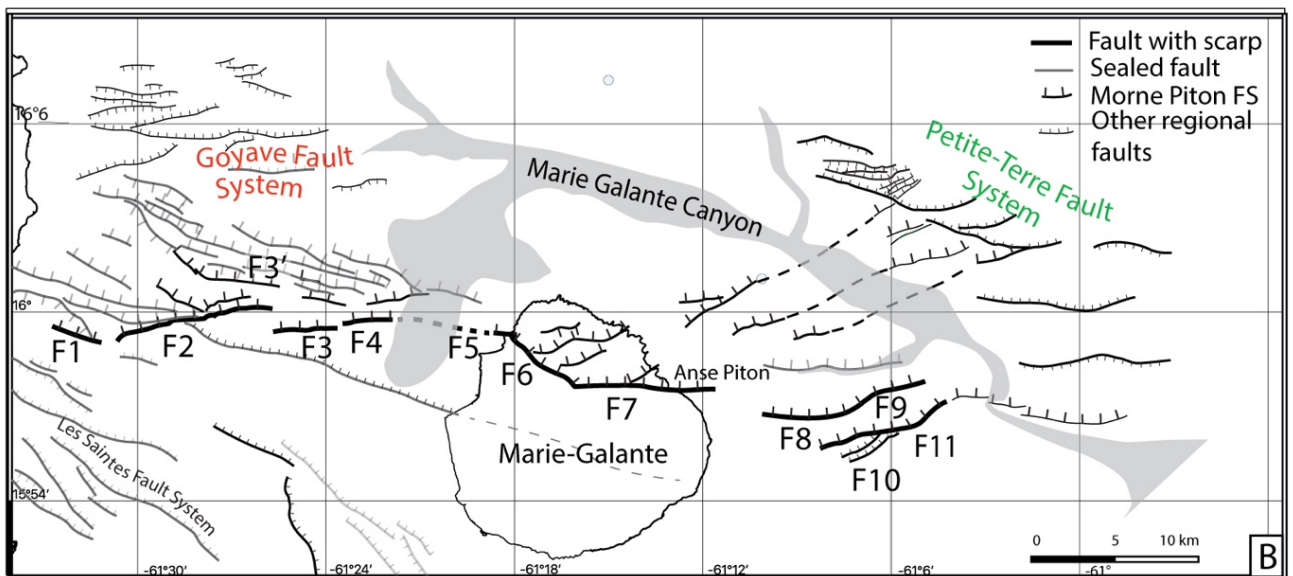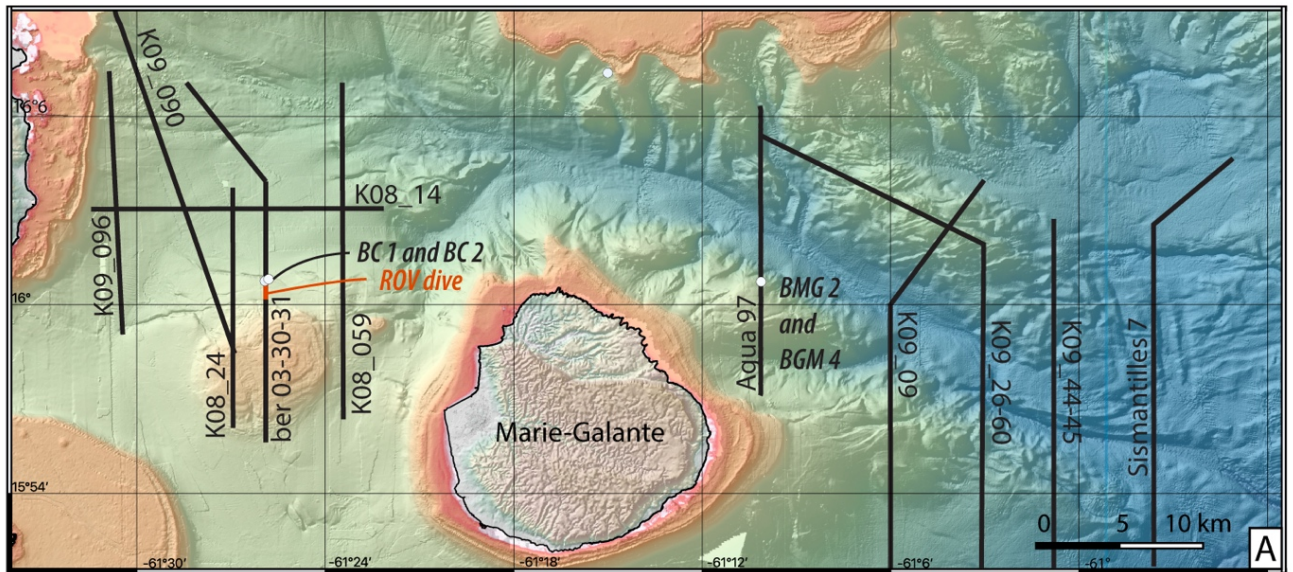
1294
1295 *Figure 3. A) High resolution (25m grid spacing) bathymetric map* [UMO16] *of the Marie-Galante Basin,*
1296 *offshore Guadeloupe and location of the seismic profiles shown on figures 4 and 5, and location of*
1297 *dredge samples used for the seismic units age calibration (Münch et al. 2013). B) Structural*
1298 *interpretation of the E-W trending Morne Piton fault system. C) A proxy for cumulative strain given*
1299 *by the graphic displaying the D (fault surface displacement) taken as the difference between the top*
1300 *and the toe of the fault scarp versus L (fault length) along the whole system.*
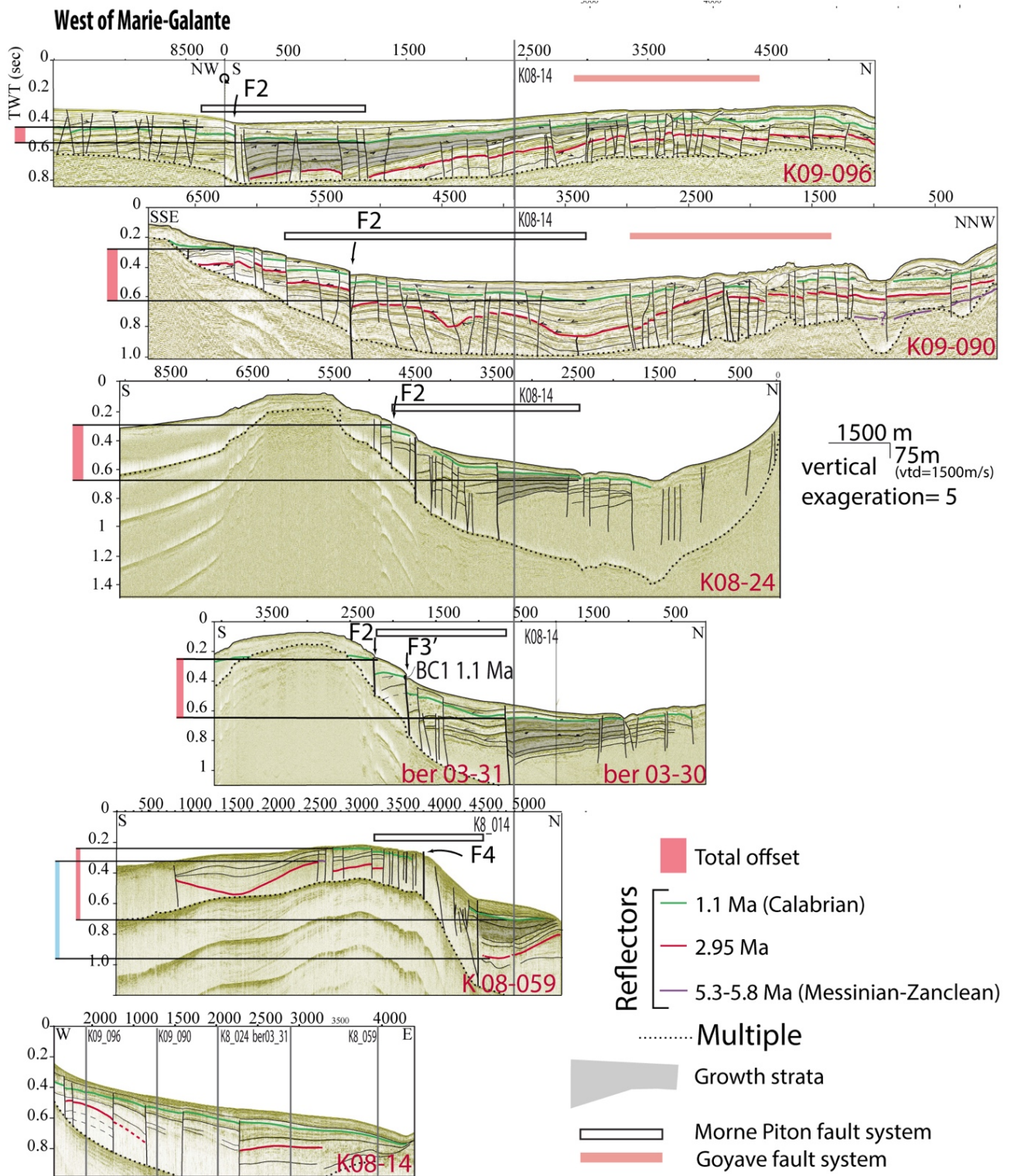
1301

Figure 4: Seismic lines West of Marie-Galante (location on Figure 3) showing the correlation across the Morne Piton fault system of the 1.29Ma unit reflector (Green) that correspond to the reflector dredged at BC1 and BC2 location along the Ber03_30-31 seismic line. The 2.95Ma Unit Boundary (Red) is correlated from seismic lines south of the Colombie Bank and Eastern Marie-Galante Basin (line K09_90 and K09_26-62 location on figure 2). Notice that the basin sedimentary slope is in the

1307   *E-W direction (parallel to line K08-14). Therefore, the initial topography of the reflectors in the N-*

1308   *S direction, across the fault system, can be neglected when measuring the offset along the seismic*

1309   *lines.*
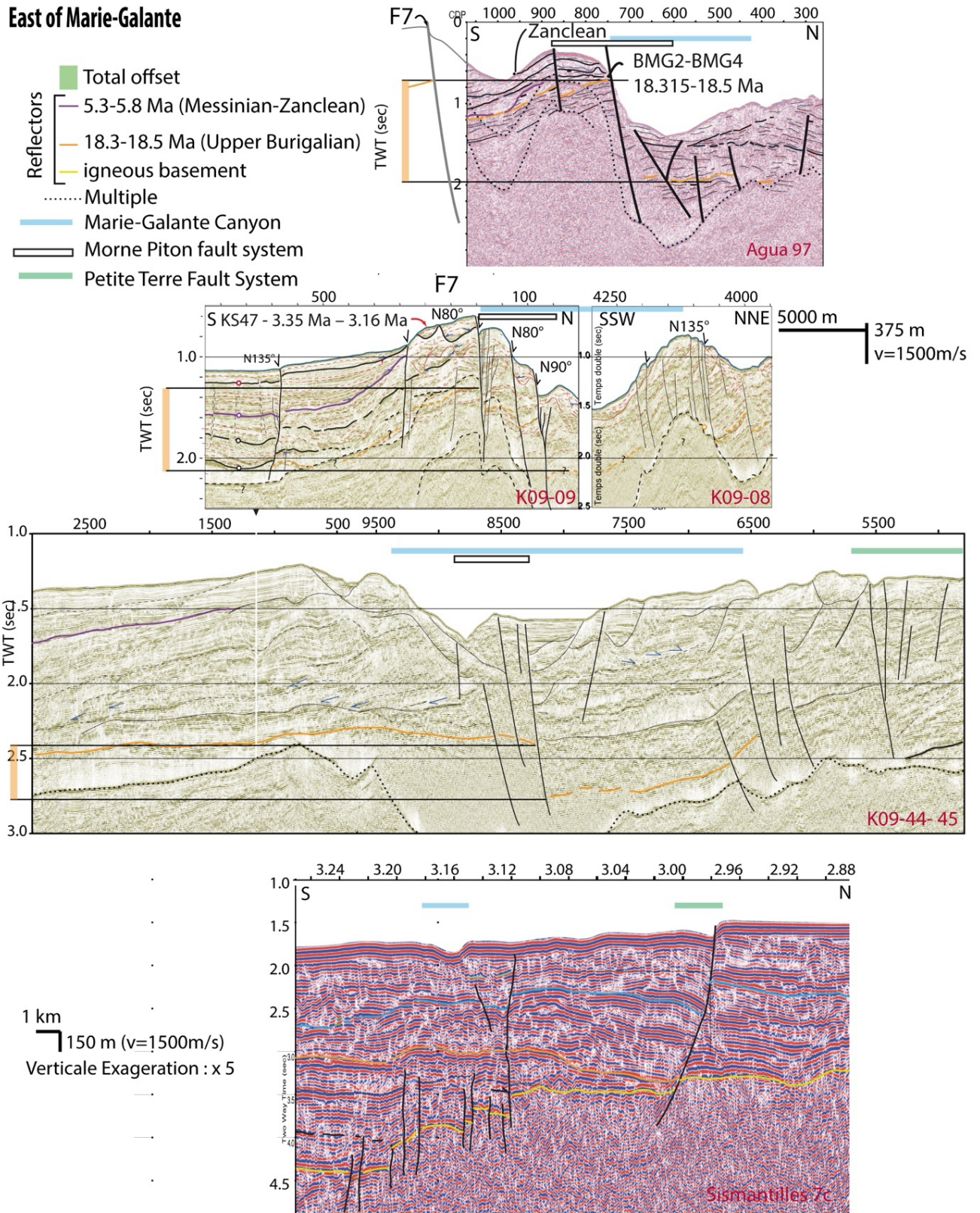
1310

Figure 5: Seismic lines east of Marie-Galante illustrate the correlation across the Morne Piton fault system of the 7 Ma (Tortonian/Messinian) MG-SB3 sequence boundary (Purple) and the 16 Ma, (Burdigalian) MG-SB2 Sequence Boundary (Orange). Seismic line location on Figure 3).
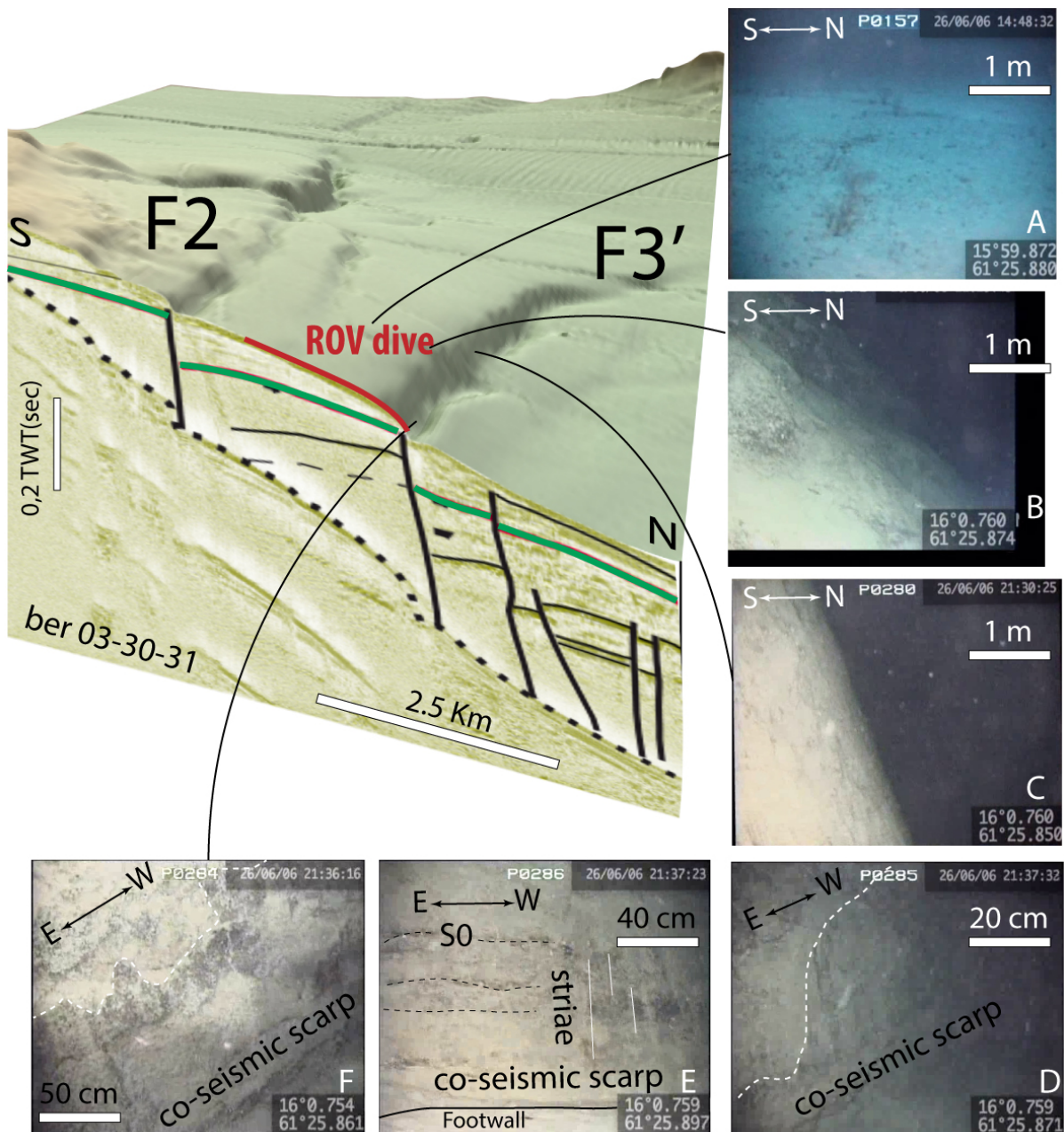
Figure 6: ROV photographs of fault identified on the seafloor along the BER03-30-31 seismic line across the F3' Morne Piton fault segment (location on Figure 3) . (A) photography of the hangingwall of F3'. The eroded F3' fault plane presents a progressive downward slope steepening (B and C) until the toe of the fault, which is marked by a characteristic co-seismic scarp with a dip slip striae (D E F). On each photograph, white numbers starting with a P is the water depth in meters Latitude is North and Longitude is West (WGS84). A B and C views show several tens square meters

 wide areas, D E F are close up showing ca 1m high escarpment just above the foot of the fault scarp

 (visible at the bottom of each photos).
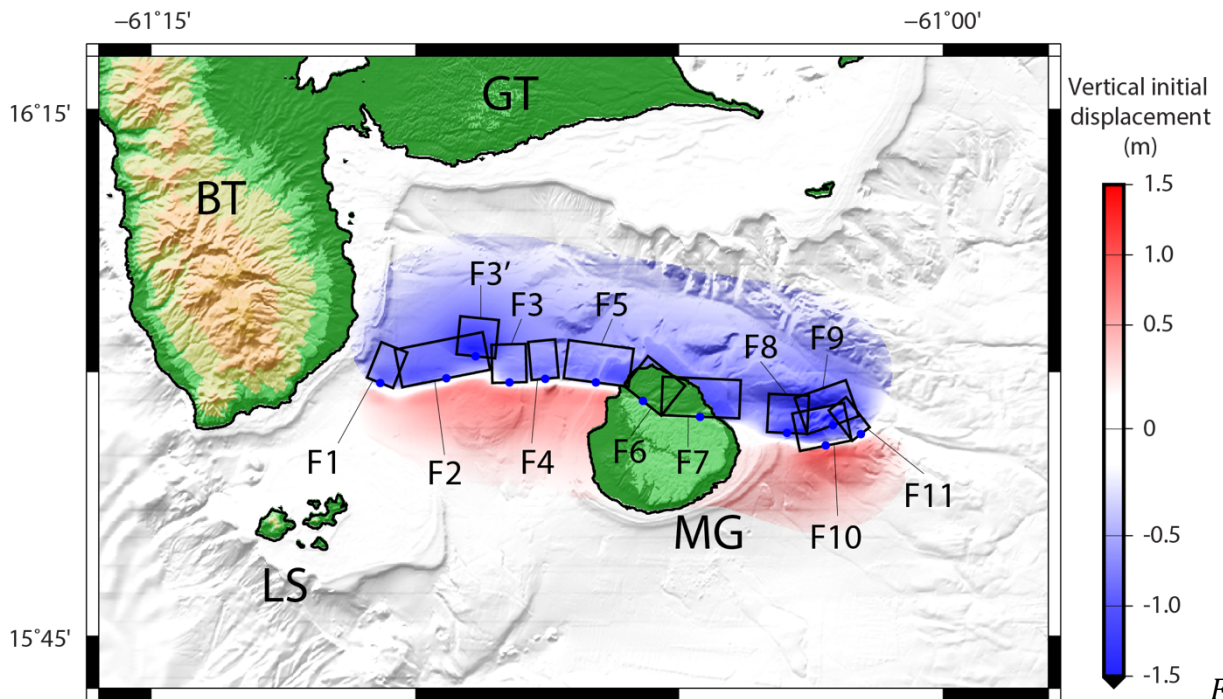
 Figure

 7: Initial surface elevation for a maximum credible scenario built with the 11 fault segments

 detailed in Table 3. Blue dots indicate the top fault center. Acronyms stand for Grande-Terre (GT),

 Basse-Terre (BT), Les Saintes (LS) and Marie-Galante (MG).
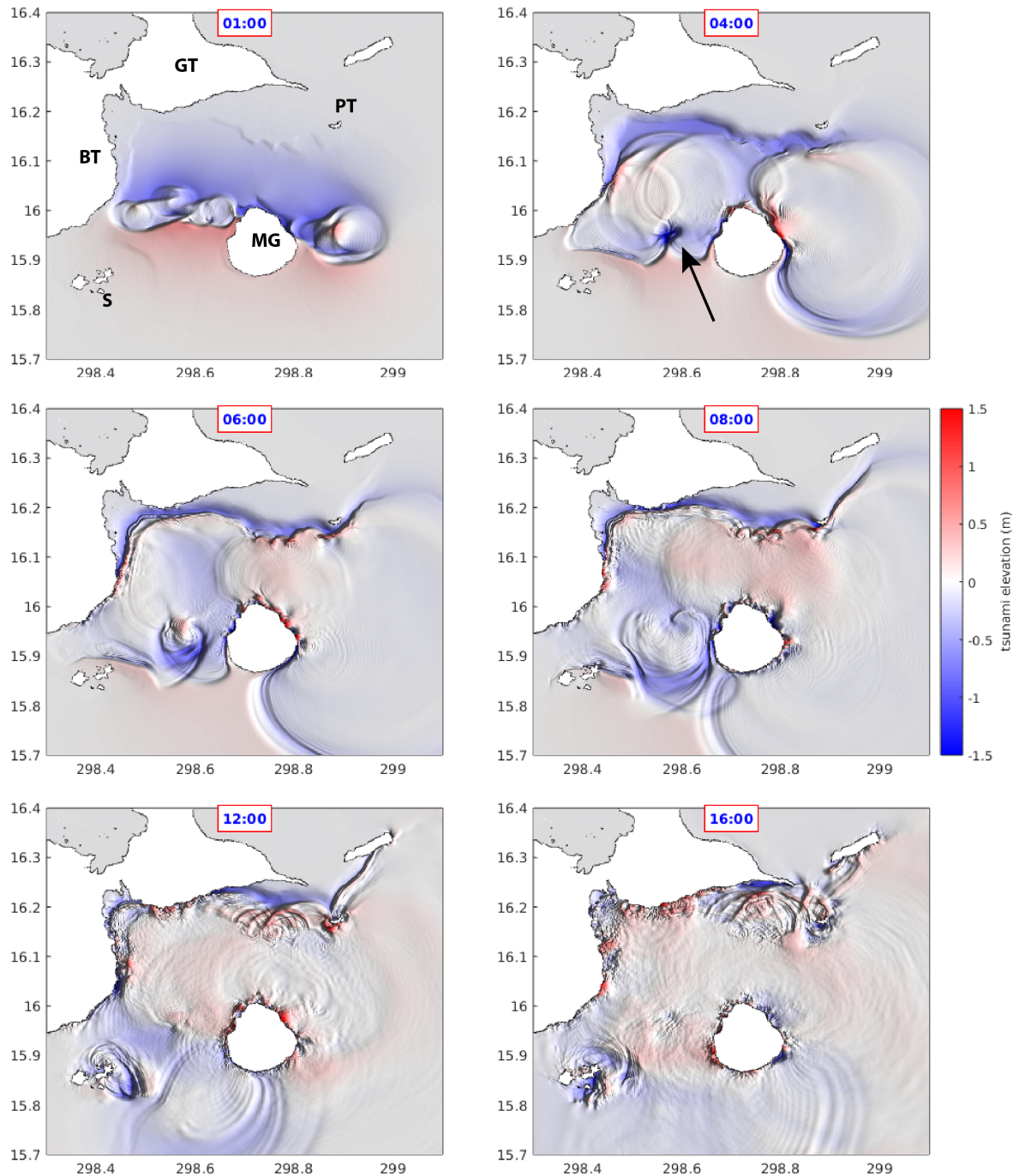
1329

1330 *Figure 8: Snapshots of tsunami elevation within the Guadeloupe Archipelago at 1, 4, 8, 6, 12 and 16*

1331 *minutes of waves propagation. Red and blue colors correspond to wave crests and troughs*

1332 *respectively. The black arrow shows the Banc Colombie shoal. BT: Basse-Terre; GT: Grande-Terre;*

1333 *S: Les Saintes; PT : Petite-Terre ; MG : Marie-Galante.*
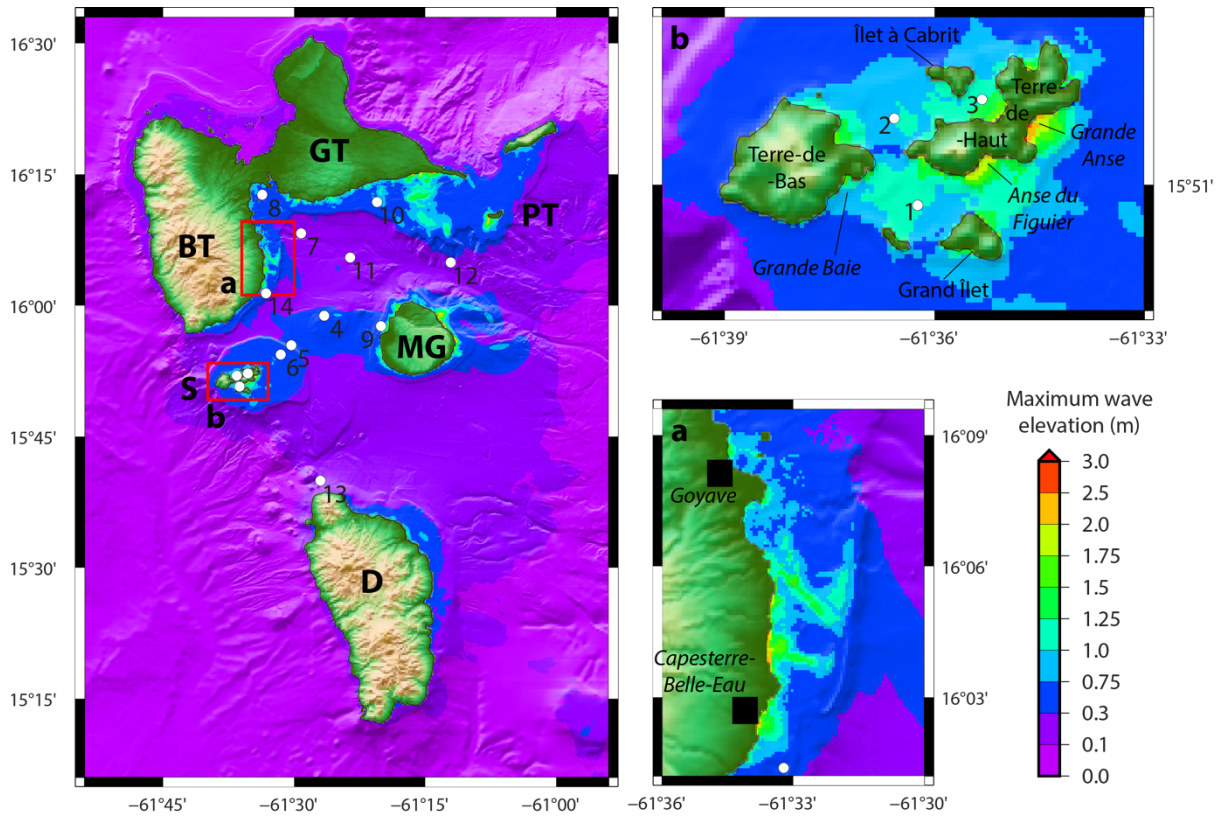
1334

Figure 9: Shadowed bathymetric map with tsunami maximum wave elevation. Numbered white dots: fourteen virtual sea-level gauges (VG) : . BT: Basse-Terre; GT: Grande-Terre; S: Les Saintes; PT : Petite-Terre ; MG : Marie-Galante ; D : Dominica. VG_4 & VG_11 are located near the fault rupture region, the VG_5 & VG_6 are near the Les Saintes Fault system. VG_1, VG_2 & VG_3 are within the Les Saintes archipelago.
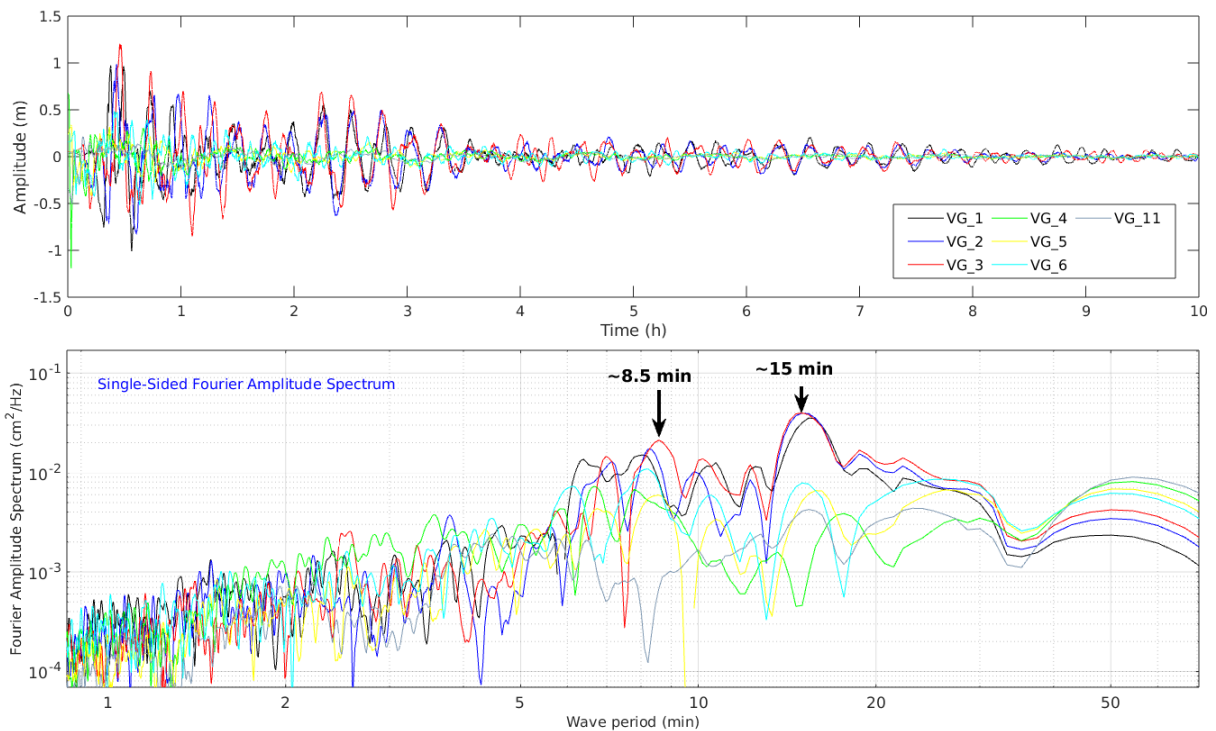
1340

1341 *Figure 10: Post-processing of virtual gauge records. Top: sea-level records at 7 different locations*

1342 *(VG 1 to 6 and VG11 – location on figure 9); bottom: single-sided Fourier amplitude spectrum. The*

1343 *blue arrows symbolize the location of the 2 peaks of period ~6.5 and 17 min.*
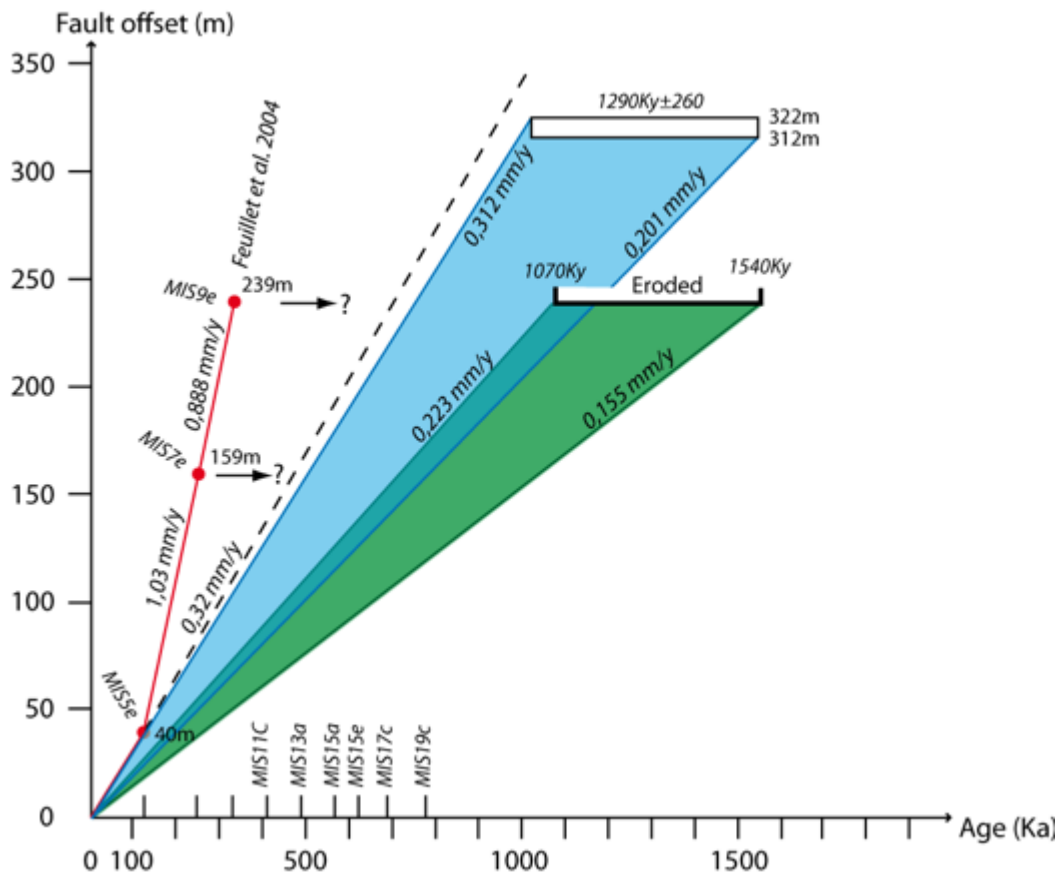
1344

1345 *Figure 11: Fault offset along the Morne Piton fault against the age of the strain marker. Red: data*

1346 *from Feuillet et al. (2004) based on absolute age of terrace T4 (MIS5e), the estimated age of terrace*

1347 *T2 (MIS7e) and the suggested age of Marie-Galante upper plateau (MIS9e). Green: strain range*

1348 *calculated using upper plateau unit age from Münch et al. (2014) (note that erosion may lower this*

1349 *estimation strain rate). Blue: strain range calculated from the fault offset of the seismic unit dated*

1350 *ca 1,2Ma along the seismic line K08-59 (green reflector on Figure 4). Dotted line indicates the 0.32*

1351 *mm·yr⁻¹ strain rate from the estimated offset of the MIS5e Terrace in Marie-Galante (Feuillet et al.*

1352 *2004).*

1353

Cruise	KaShallow 1	KaShallow 2	Aguadomar	SismAntilles	GEOBERYX03 SISM BGM
Seismic source	1000 J sparker	35-45 in3 GI Airguns array	45-105 in3 Two GI Airguns	4400 in3 Airguns array.	1000 J sparker
Peak frequency (far field)	250-400Hz	40-70Hz	30-50Hz	15-20Hz	250-400Hz
Number of traces	6 traces	72 traces	6 traces	360 traces	6 traces
Fold coverage	3/6 fold	9/18 fold	3 fold	30 fold	3/6 fold
Inter CDP distance	4 m	3.125 m	4 m	6,25 m	4 m

1354

1355 *Table 1: Main acquisition parameters of the seismic data shown in this study (Figures 4 and 5).*

1356

1357

Profile Name sorted from East to West	Age	Uncertainty (Ma)	horizon depth in the footwall (stwt) water	horizon depth in the footwall (stwt) rock	horizon depth in the hangingwall (stwt) water	horizon depth in the hangingwall (stwt) rock	horizon depth in the footwall (m) max [V en m/s 2500]	horizon depth in the hanging wall (m) max [V en m/s 2500]	horizon depth in the footwall (m) min [V en m/s 2000]	horizon depth in the hanging wall (m) min [V en m/s 2000]	TOTAL OFFSET (m) max [V en m/s 2500]	TOTAL OFFSET (m) min [V en m/s 2000]	Strain rate (mm/years) min	max	Average	nty	Interval strain rate (mm/yrs)
K09-44-45 –MG-SB2	16	1	1,575	0,83	1,575	1,2	2 212,5	2 700,0	2 006,3	2 396,3	487,5	390,0					
since inception	7	1,5											0,046	0,089	0,067	0,030	
K09_08-09 –MG-SB2	16	1	0,595	0,91	1,27	0,9	1 577,5	2 052,5	1 351,3	1 832,5	475,0	481,3					
since inception	7	1,5											0,057	0,086	0,071	0,021	
Agua 97 –MG-SB2	16	1	0,05	0,72	1,36	0,6	937,5	1 770,0	757,5	1 620,0	832,5	862,5					
since inception	7	1,5											0,101	0,151	0,126	0,035	0,07
UB4	2,95	0,05	0,23	0,09	0,59	0,4	285,0	905,0	262,5	812,5	620,0	550,0	0,183	0,214	0,199	0,022	0,16
K08-059	1,29	0,26	0,22	0,02	0,5	0,1	190,0	512,5	185,0	485,0	322,5	300,0	0,194	0,313	0,253	0,085	0,25
Ber 03-31	1,29	0,26	0,21	0,04	0,53	0,1	207,5	522,5	197,5	497,5	315,0	300,0	0,194	0,306	0,250	0,079	
K08-24	1,29	0,26	0,25	0,04	0,6	0	237,5	487,5	227,5	480,0	250,0	252,5	0,163	0,243	0,203	0,056	
K09-090	1,29	0,26	0,33	0,02	0,49	0,1	272,5	530,0	267,5	497,5	257,5	230,0	0,148	0,250	0,199	0,072	
K09-096	1,29	0,26	0,32	0,12	0,44	0,1	390,0	505,0	360,0	470,0	115,0	110,0	0,071	0,112	0,091	0,029	

1358 *Table 2: Measured offset of seismic reflectors across the Morne Piton fault system and calculated*

1359 *total vertical strain rates. See text for the ages estimate. Seismic reflectors depth on each side of the*

1360 *fault system is measured in time (stwt – second two way time) and converted in depth in using water*

1361 *velocity (1500m/s) and two end-member velocities for the sediment (see text for explanation),*

1362 *providing a minimum and a maximum offset value. The minimum strain rate is obtained from the*

1363 *ratio between the min offset and the max age bound of the reflector and vice versa.*

1364

Fault segment	Lon (°)	Lat (°)	Length (m)	Width (m)	Top of the fault plane depth (m)	Strike (°)	Dip (°)	Rake (°)	Slip (m)
F1	-61.5335	15.98987	2838	12500	500	111	75	-90	1.89
F2	-61.4708	15.994	9070	12500	500	78	75	-90	1.89
F3'	-61.4428	16.01503	3918	12500	500	95	75	-90	1.89
F3	-61.4108	15.99009	3474	12500	500	88	75	-90	1.89
F4	-61.377	15.99367	2735	12500	500	84	75	-90	1.89
F5	-61.3287	15.99021	6623	12500	500	97	75	-90	1.89
F6	-61.2846	15.97275	4813	12500	500	128	75	-90	1.89
F7	-61.2301	15.95767	7904	12500	500	92	75	-90	1.89
F8	-61.1477	15.94221	4052	12500	500	92	75	-90	1.89
F9	-61.1042	15.94958	5495	12500	500	70	75	-90	1.89
F10	-61.111	15.93014	5336	12500	500	78	75	-90	1.89
F11	-61.0777	15.94126	2228	12500	500	52	75	-90	1.89

1365

1366 *Table 3: Parameters used for the tsunami source simulation of a rupture along the multisegment*

1367 *fault presented in figure 7.*

1368